

Hippocampal mechanisms resolve competition in memory and perception

Serra E. Favila and Mariam Aly

Department of Psychology, Columbia University, New York, NY, 10027

Please address correspondence to: Serra Favila (sef2177@columbia.edu)

ORCID:

Serra Favila: <https://orcid.org/0000-0003-1528-2875>

Mariam Aly: <https://orcid.org/0000-0003-4033-6134>

Conflict of Interest: The authors declare no competing interests.

Author Contributions: Conceptualization, S.E.F. and M.A.; Methodology, S.E.F. and M.A.; Software, S.E.F.; Investigation, S.E.F.; Writing – Original Draft, S.E.F. and M.A.; Writing – Review & Editing, S.E.F. and M.A.; Funding Acquisition, M.A.; Supervision, M.A.

Acknowledgements: This work was funded by an NSF CAREER Award (BCS1844241) to M.A. S.E.F was supported by an NIH D-SPAN K00 Award (K00EY031607). We thank Shelton Brister and Kaylee Wang for their assistance with data collection and the Alyssano Group and Brice Kuhl for their helpful feedback on this project.

Abstract

Behaving adaptively requires selection of relevant memories and sensations and suppression of competing ones. We hypothesized that these mechanisms are linked, such that hippocampal computations that resolve competition in memory also shape the precision of sensory representations to guide selective attention. We leveraged fMRI-based pattern similarity, receptive field modeling, and eye tracking to test this hypothesis in humans performing a memory-dependent visual search task. In the hippocampus, differentiation of competing memories predicted the precision of memory-guided eye movements. In visual cortex, preparatory coding of remembered target locations predicted search successes, whereas preparatory coding of competing locations predicted search failures due to interference. These effects were linked: stronger hippocampal memory differentiation was associated with lower competitor activation in visual cortex, yielding more precise preparatory representations. These results demonstrate a role for memory differentiation in shaping the precision of sensory representations, highlighting links between mechanisms that overcome competition in memory and perception.

Introduction

At any given moment, we are faced with multiple sensations, memories, and thoughts that compete to take control of our behavior. Behaving adaptively requires resolution of this competition, to focus on only those memories or external events that are relevant in the current context. Multiple cognitive domains, from perception to memory, have highlighted the necessity of selecting between competing representations for generating adaptive behavior. Yet, these aspects of cognition are largely studied separately, leading to assumptions that the way competition is resolved in memory is fundamentally different from how it is resolved in perception. An alternative possibility is that the computational principles that overcome competition in memory and perception are closely intertwined, such that mechanisms that resolve competition in memory also shape the precision of online perceptual behavior.

Within the field of visual perception, it has long been appreciated that limited processing capacity requires humans to make moment-by-moment decisions about what information to attend to and what to ignore (Carrasco, 2011; van Moorselaar & Slagter, 2020). These competitive interactions have been well-characterized in behavior and within visual cortex, where attention is known to modulate the strength and precision of stimulus representations (McAdams & Maunsell, 1999; Somers et al., 1999; Liu et al., 2005; Sprague & Serences, 2013; Desimone & Duncan, 1995; Kastner & Ungerleider, 2000). Separately, within the field of episodic memory, a considerable amount of research has focused on the role of the hippocampus in discriminating similar memories such that competition between them is minimized. Computational models (Norman et al., 2006; Ritvo et al., 2023) and fMRI studies in humans (Hulbert & Norman, 2015; Schlichting et al., 2015; Favila et al., 2016; Chanales et al., 2017; Molitor et al., 2020; Wanjia et al., 2021) suggest that in addition to orthogonalizing memories automatically, the hippocampus further differentiates memories that compete during retrieval. This differentiation is thought to be an adaptive response to competition that minimizes future memory interference. Although competitive interactions in attentional selection and memory are typically studied independently, there is reason to expect that these mechanisms are linked via the hippocampus. Prior work has shown that the hippocampus is involved in online attentional behavior (Chun & Phelps, 1999; Summerfield et al., 2006; Hannula & Ranganath, 2009; Aly & Turk-Browne, 2016; Córdova et al., 2019; Ruiz et al., 2020), codes for gaze-related variables at the single cell level (Rolls, 1999; Killian et al., 2012; Mao et al., 2021), and interacts with visual and oculomotor systems in support of memory-guided attention (Stokes et al., 2012; Günseli & Aly, 2020; Ryan et al., 2020; Poskanzer & Aly, 2023; Hutchinson & Turk-Browne, 2012; Aly & Turk-Browne, 2017). Combining these disparate literatures, we hypothesized that hippocampal mechanisms that differentiate competing memories would reduce activation of competing features in visual cortex and support efficient and precise attentional selection.

To test these predictions, we designed a novel task that required participants to rely on competing memories to guide visual attention. Participants first acquired pairs of competing memories, which consisted of two highly similar scenes that were associated with distinct spatial

locations. Then, while they were scanned with fMRI, participants performed a difficult visual search task. Critically, the search task was structured such that participants could use memories from the previous session to predict the location of upcoming search targets. We recorded participants' eye movements continuously during this task, allowing us to assess the efficiency of attentional guidance. Using a combination of pattern similarity and population receptive field modeling approaches to analyze the fMRI data, we measured: 1) differentiation of competing memories in the hippocampus; 2) preparatory representations of target and competitor locations in visual cortex prior to search onset; and 3) the relationship between hippocampal and visual cortical representations and their impact on behavior.

Results

Competitive scene-location learning

Human participants ($N = 32$) took part in a two session experiment that spanned consecutive days. In session 1, participants learned 24 scene-location associations. To create memory competition, the 24 scenes consisted of 12 pairs of highly similar images (pairmates; Fig. 1A). Each scene was associated with a spatial location, which we will refer to as its target location (Fig. 1B). There were 8 possible locations arranged in a circle, equidistant from the center of the screen and equidistant from each other. Pairmates were never associated with the same location. Participants were first exposed to the scenes without their associated locations and then performed interleaved study and test blocks on the scene-location associations (Fig. 1C). During study blocks, participants were presented with the scene-location associations, one at a time. During test blocks, participants were cued with one of the scene images and asked to respond by making a memory-guided saccade to the associated target location on a blank display. To succeed at this task, participants had to discriminate between scene pairmates such that they could respond with the target location associated with the cued scene and avoid responding with the competitor location associated with the cued scene's pairmate.

To evaluate memory, we measured the angular error between participants' final saccade end point and three relevant locations along the circle of studied locations: 1) the target location; 2) the competitor location; and 3) a control location an equal distance away from the target as the competitor. It was not possible to define a control location when target-competitor distances were 180 degrees, and thus these trials were excluded for all control vs. competitor location comparisons. We assigned a participant's final saccade to one of these three locations if it was closer to that location than to any of the other studied locations (i.e. if the angular error between the saccade end point and the center of the relevant location was less than 22.5 degrees). To establish whether participants experienced memory competition, we first examined the relative probability of saccades to the competitor and control locations. Across all test trials, participants were significantly more likely to make responses to the competitor than to the control location ($t_{31} = 4.74$; $p < 0.0001$; Fig. 1D), validating the presence of competition. We then confirmed that learning occurred during the session by comparing target and competitor response probabilities

between the first and last test presentation. The relative probability of these responses changed reliably over the session (target/competitor \times first/last interaction: $F_{1,31} = 95.8$; $p < 0.0001$; Fig. 1E). Participants made significantly more responses to the target location from the first to the last test presentation (first = 37.9%; last = 67.8%; $t_{31} = 9.82$; $p < 0.0001$) and significantly fewer responses to the competitor (first = 12.4%; last = 4.9%; $t_{31} = -5.60$; $p < 0.0001$). Thus, participants successfully acquired the scene-location associations in the first experimental session, overcoming interference from memory competitors to do so.

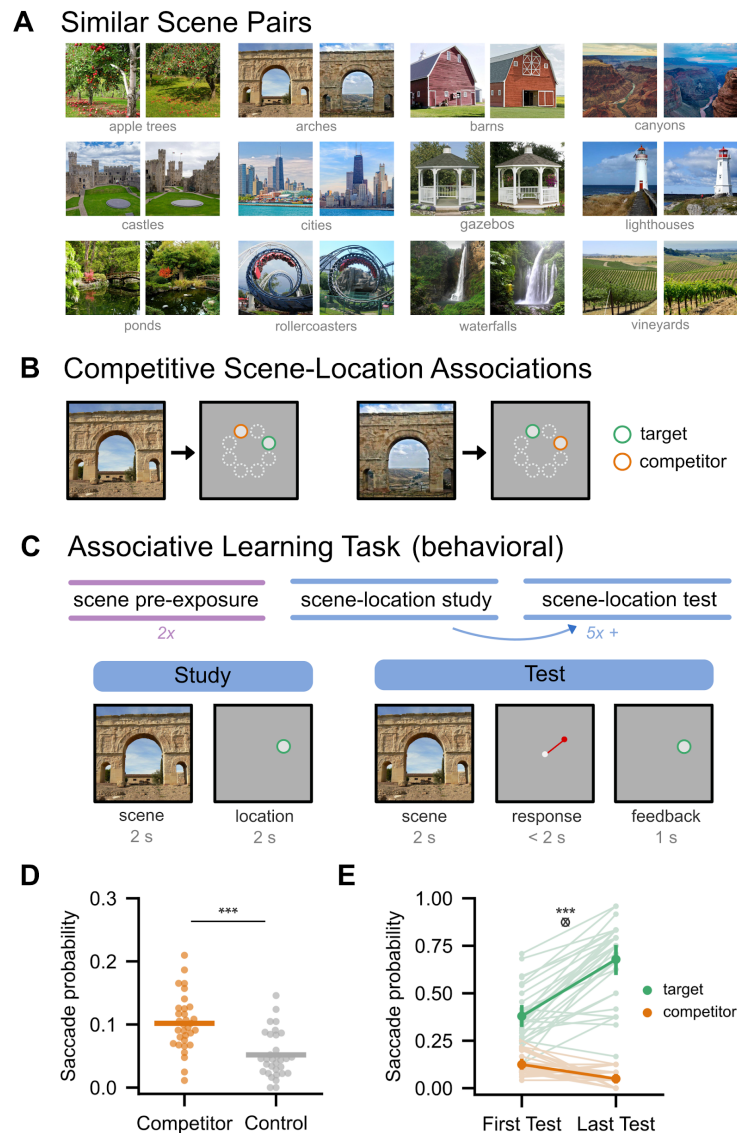


Figure 1. Experimental design and behavioral data from competitive learning task (session 1). (A) Twelve pairs of highly similar scenes (“paimates”) were used throughout the experiment. (B) Each scene was associated with one of eight possible spatial locations, which we refer to as that scene’s target location. The paimate structure of the scenes was intended to create memory competition, such that participants may accidentally bring to mind the target location of the similar scene. We refer to this location as the competitor location. The competitor location is highlighted for visualization purposes only; participants saw each image paired with its target location only. (C) Participants (N=32) were first exposed to all 24 scenes two times each. They then acquired the scene-location associations through interleaved study and test blocks. During study

trials, participants intentionally encoded the scene-location pairs. During test trials, participants were cued with a scene and after a brief central fixation interval (not shown), made a memory-guided saccade to the recalled location. Participants were shown the correct location at the end of the trial as feedback. **(D)** Participants were more likely to make saccades to the competitor location than to a distance-matched control location ($t_{31} = 4.74$, $p < 0.0001$), establishing the presence of memory competition. Dots represent individual participant data and horizontal lines represent the across-participant mean. **(E)** Participants' memory improved over the course of the session, reflected by more frequent saccades to the target location and less frequent saccades to the competitor location ($F_{1,31} = 95.8$, $p < 0.0001$). Light points and lines represent individual participant data. Dark points and error bars represent the across-participant mean and bootstrapped 95% confidence interval.

Memory-guided visual search behavior

In session 2, participants performed a memory-guided visual search task while being scanned with fMRI. On every trial, participants were presented with a scene image that contained a distortion (Fig. 2A; see *Methods/Scene Distortions*). Participants' task was to find this distortion as quickly and accurately as possible by moving their eyes and holding fixation once they found it. Critically, we embedded structure in the task that allowed participants to use the memories they formed in session 1 to boost their performance. Participants were told that the location associated with a given scene from session 1 was a reliable predictor of the distortion location on the *next* trial. Brief scene presentation and a long intertrial interval encouraged participants to engage in memory-based prediction to allocate attention optimally on the next trial. There were three critical task conditions (Fig. 2B). On valid trials (75% of trials), the distortion was placed in the predicted target location. On invalid trials (12.5% of trials), the distortion was placed in the competitor location. On no-prediction trials (12.5% of trials), the distortion was placed randomly in one of the 8 possible locations used in the experiment (Fig. 1B). These no-prediction trials always followed trial-unique novel scenes that had no associated location that participants could recall.

To evaluate whether participants were using memory to improve search performance, we examined participants' first saccade after search onset across the three conditions. We calculated the angular error between participants' first saccade end point and the center of the distortion location on each trial and scored this saccade as accurate if it was closer to the distortion than to any of the other 7 possible locations (< 22.5 degrees of angular error). We found highly reliable differences in accuracy across the three conditions (valid = 45.4%; no-prediction = 21.5%; invalid = 16.9%; $F_{2,62} = 78.7$, $p < 0.0001$; Fig. 2C). Consistent with standard attentional cueing effects, participants were more likely to make accurate first saccades on valid trials compared to no-prediction trials ($t_{31} = 8.72$, $p < 0.0001$) and invalid trials ($t_{31} = 9.74$, $p < 0.0001$). Participants were also less likely to make accurate first saccades on invalid trials than on no-prediction trials ($t_{31} = -3.44$, $p = 0.0016$). Relative to the first saccade, the final saccade of the search interval was more accurate in every condition (valid = 64.9%; no-prediction = 44.5%; invalid = 37.8%). However, condition differences were still highly significant for the final saccade ($F_{2,62} = 65.9$, $p < 0.0001$), with valid performance highest and invalid performance lowest (all pairwise comparisons significant at $p < 0.0001$). To determine whether memory competition remained during visual search, we evaluated whether participants sometimes used the competing memory to guide their

attention. To that end, we looked at the distribution of first saccades on valid trials, in which the distortion appeared at the target location. As expected, the first saccade on these trials was frequently near the target (and distortion) location (Fig. 2D). Critically, more first saccades were close to the competitor location than to a control location equally far from the target ($t_{31} = 7.59$, $p < 0.0001$; Fig. 2E). This pattern of behavior suggests that interference between the similar scenes created competition in attention and memory, because it was not behaviorally advantageous to make a first saccade to the competitor location (statistically, the target location was more likely to contain the distortion and did indeed contain the distortion on these valid trials).

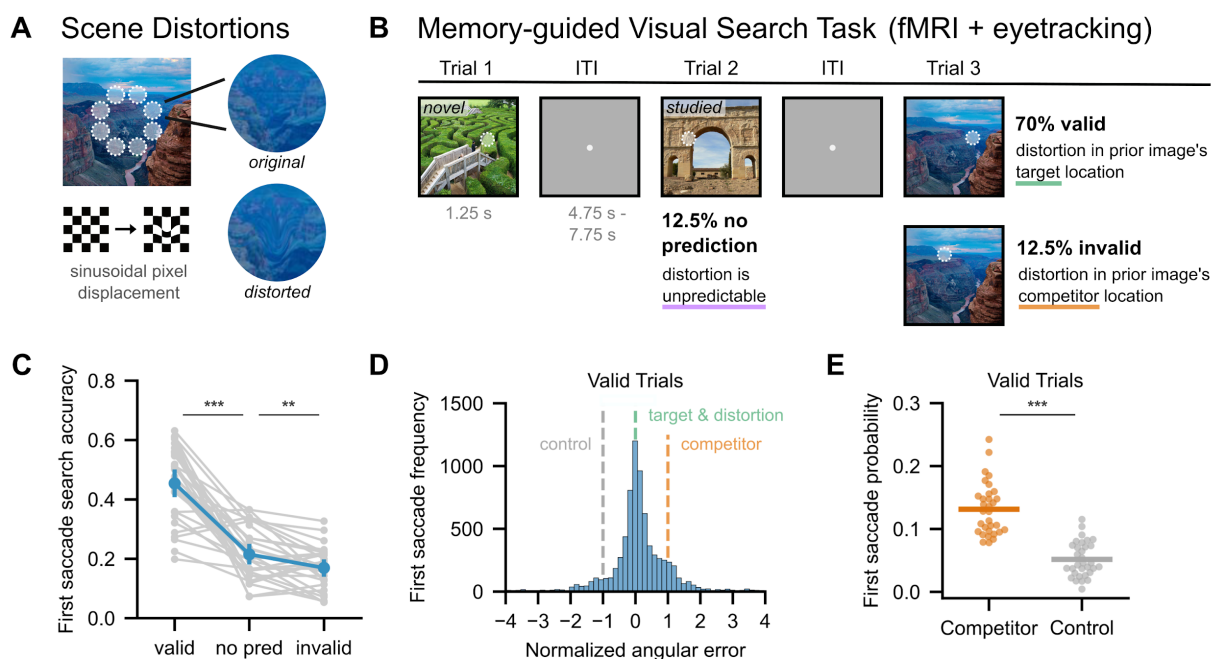


Figure 2. Experimental design and behavioral data from memory-guided visual search task (session 2). (A) Scene distortions were created by applying a sinusoidal pixel displacement to a local patch of the image. (B) Participants performed a memory-guided visual search task while being scanned. On each trial of the task, a scene with one local distortion was presented (highlighted with a white circle for visualization only). Participants were instructed to search for the distortion by moving their eyes. Critically, participants could predict the location of the distortion on the upcoming trial by recalling the target location associated with the previous image. We placed the distortion in the predicted target location on 75% of trials (valid trials) and in the competitor location on 12.5% of trials (invalid trials). 12.5% of trials followed trial-unique novel images (no-prediction trials, i.e., distortion location is unpredictable). (C) Relative to the no-prediction condition, participants' first saccade was more accurate in the valid condition ($t_{31} = 8.72$, $p < 0.0001$) and less accurate in the invalid condition ($t_{31} = -3.44$, $p = 0.0016$), indicating that participants were using memory to guide their search performance. Grey points and lines represent individual participant data. Blue points and error bars represent the across-participant mean and bootstrapped 95% confidence interval. (D) The distribution of first saccade angular errors on valid trials. Angular errors are normalized by the target-competitor distance such that $x = 0$ is the target (and distortion) location, $x = 1$ is the competitor location, and $x = -1$ is a control location the same distance from the target as the competitor. While first saccades near the target location were most likely, the distribution is asymmetric toward the competitor. (E) First saccade probabilities are plotted separately for the competitor location ($x = 1$ in (D)) and the control location ($x = -1$ in (D)). Participants were significantly more likely to make their first saccade to the competitor location than to the control location on

valid trials ($t_{31} = 7.59$, $p < 0.0001$), suggesting that memory competition from the prior session persisted into the search task. Dots represent individual participant data and horizontal lines represent the across-participant mean.

Together, these results confirm that participants performed accurately on the search task but nevertheless experienced memory competition. To explore whether search variability was related to individual differences in memory, we compared search performance in session 2 to learning in session 1. Across-participant variance in search performance on valid trials was strongly predicted by variance in final memory performance on day 1 (proportion of saccades near target location on day 1 vs. day 2, $r_{30} = 0.56$, $p = 0.0009$). Furthermore, the degree of memory competition experienced by participants on day 1 predicted competition on day 2 (proportion of saccades near competitor location on day 1 vs. day 2, $r_{30} = 0.40$, $p = 0.025$). These results validate the importance of memory, and the resolution of memory competition, for visual search performance.

Differentiation of competing scenes in the hippocampus

We focused our fMRI analyses of the memory-guided search task on two regions of interest: 1) the hippocampus, which is critical for resolving memory competition (O'Reilly & McClelland, 1994; Shapiro & Olton, 1994; Wanjia et al., 2021), and 2) early visual cortex, whose representations are biased in favor of attentional targets (Gandhi et al., 1999; Somers et al., 1999; Liu et al., 2005). For each participant, we defined the hippocampus (HIPPO) anatomically in native space. To define early visual cortex (EVC), we combined areas V1, V2, and V3, each of which were defined functionally in native space using data from a separate retinotopic mapping task (see *Methods/Regions of Interest*).

First, we sought to establish that the hippocampus differentiates competing memories, consistent with prior work. To investigate this, we estimated the average pattern of BOLD activity evoked by every scene image in the search task (24 paired scenes and 56 novel scenes; see *Methods/Pattern Similarity Analyses*). For each of the 12 scene pairs, we computed the neural pattern similarity (z-transformed Pearson correlation) of the pairmate images (e.g. arch 1 and arch 2, *pairmate pattern similarity*; Fig. 3A). For each scene pair, we also computed the average pattern similarity between each of the pairmates and all non-pairmate images (e.g. arch 1 and barn 2, *nonpairmate pattern similarity*). Pattern similarity with novel images was excluded from the nonpairmate average to control for image familiarity. For each scene pair, we then computed the difference between pairmate and nonpairmate pattern similarity, which we refer to as “scene pair pattern similarity”. Critically, this difference measure indicates the degree to which pairmates are differentiated in a given brain region, controlling for the average similarity across images in that region. Higher values indicate that pairmates are relatively more similar to each other than they are to other images, whereas lower values indicate that pairmates are relatively more differentiated from each other compared to other images. If the hippocampus resolves competition between similar memories, its representations of pairmates should be relatively differentiated compared to representations in visual cortex, an input region not thought to play a role in competition resolution. To test this, we compared scene pair pattern similarity in the

hippocampus and visual cortex. Consistent with this prediction, scene pair pattern similarity values differed between these regions, with lower scene pair pattern similarity values in the hippocampus than in visual cortex (HIPP: -0.018; EVC: 0.022; $t_{31} = -10.2$, $p < 0.0001$; Fig. 3B). Thus, as in prior work (Favila et al., 2016; Wanjia et al., 2021), the hippocampus differentiated similar memories.

A Scene pair pattern similarity

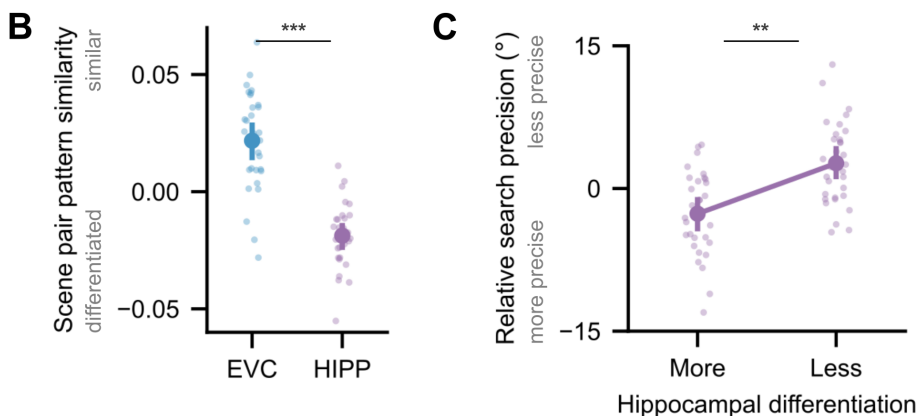
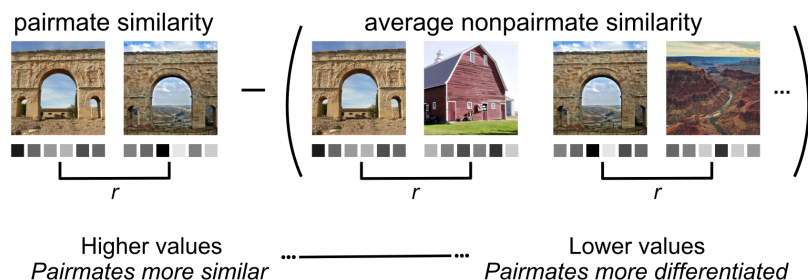


Figure 3. Differentiation of competing scenes in the hippocampus predicts the precision of memory-guided eye movements. (A) For every pair of similar scenes, we computed scene pair pattern similarity as the difference between paimate similarity (e.g. arch 1 and arch 2) and average nonpaimate similarity (e.g. arch 1 and barn 2). Under this measure, lower values indicate that paimates were relatively more differentiated from each other compared to other scenes. (B) We compared average scene pair pattern similarity in early visual cortex (EVC; defined as V1, V2, and V3) and the hippocampus (HIPP). Consistent with prior work, competing scenes were more differentiated in the hippocampus relative to visual cortex ($t_{31} = -10.2$, $p < 0.0001$). Small dots represent individual participant data. Large dots and error bars represent the across-participant mean and bootstrapped 95% confidence interval. (C) The strength of scene pair differentiation in the hippocampus was related to memory-guided search precision. Scene pairs that were more differentiated in the hippocampus were followed by more precise first saccades to the associated target locations on the next trial ($t_{31} = -3.46$, $p = 0.0016$). Precision values (angular error between first saccade endpoint and the distortion on valid trials) are centered within participants for visualization. Small dots represent individual participant data. Large points and error bars represent the across-participant mean and bootstrapped 95% confidence interval.

Because our task requires discrimination between competing scenes to make an accurate memory-guided saccade on the next trial, we hypothesized that the magnitude of memory differentiation in the hippocampus would predict the precision of upcoming saccades within a participant. For every participant and scene pair, we computed upcoming saccade precision as

the average error between the first saccade endpoint and the distortion location on valid trials following the presentation of either scene pairmate of interest. Scene pairs that were more differentiated in the hippocampus (i.e. with lower scene pair pattern similarity) were followed by more precise saccades than scene pairs that were less differentiated ($t_{31} = -3.46$ $p = 0.0016$; Fig. 3C). There was no relationship between differentiation in visual cortex and saccade precision ($t_{31} = -1.24$ $p = 0.22$). These results show the importance of hippocampal differentiation for rapid attentional behavior guided by memory, allowing us to investigate interactions between hippocampal differentiation and visual cortical representations supporting attention.

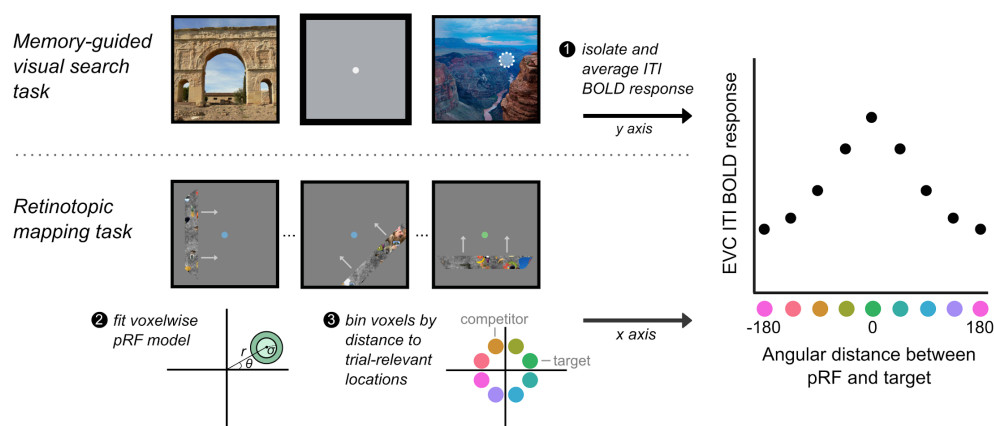
Preparatory target and competitor location coding in visual cortex

Having established that competition between similar memories is largely overcome in behavior, and that this resolution of competition is reflected in hippocampal coding, we next sought to understand how these memories were used to benefit visual search. Our search task was designed so that participants could use memory to predict the location of the upcoming distortion during the blank inter-trial interval (ITI). Because early visual cortex contains maps of the visual field, and because these maps can be activated in a top-down manner (Kosslyn et al., 1995; Kastner et al., 1999; Breedlove et al., 2020; Favila et al., 2022), we hypothesized that participants' location predictions during the ITI would be represented by spatially-organized activity within these maps. Given how critical memory-based prediction was to task performance (see Fig. 2C), we also hypothesized that preparatory location coding in visual cortex would be associated with search success on the next trial.

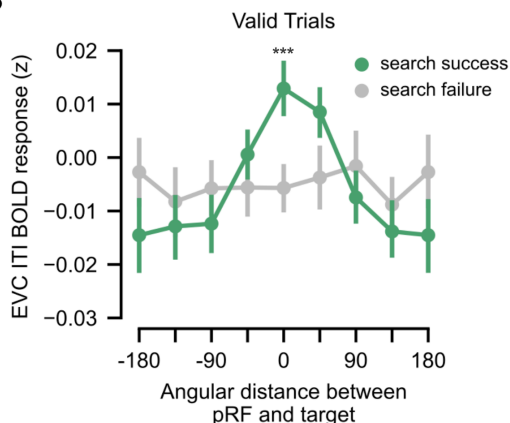
To test this hypothesis, we took advantage of models that were developed to characterize the spatial organization of visually-evoked fMRI signals. Using data from a separate retinotopic mapping task, we estimated the best-fitting population receptive field (pRF) for each voxel in a participant's brain (Fig. 4A and see *Methods/pRF Model Fitting*). This pRF represents the location and extent in the visual field of that voxel's maximal response to visual stimulation. We used the pRF parameters to isolate voxels in early visual cortex (EVC; defined as V1, V2, and V3) with responsiveness to the 8 possible target locations. We then examined the BOLD response in these EVC voxels during the blank ITI of the search task, after regressing out task-evoked activity to remove confounding effects of the visual response from the preceding trial (Fig. 4A and see *Methods/Visual Cortex Preparatory Responses*). Voxels were binned according to the distance between their pRF and the target memory location on the upcoming trial; ITI responses were then separately averaged within each bin and separately for upcoming search successes and failures. We focused on valid trials, in which memory yielded accurate predictions; thus, search successes were trials in which the search concluded at the distortion (also the target memory location) and search failures were all other trials. This procedure generated two neural representations of *predicted* locations during the ITI, one for upcoming search successes and one for upcoming search failures. Consistent with our hypothesis, visual cortex representations differed for search successes and failures (angular distance from target \times search success/failure interaction: $F_{7,217} = 3.03$, $p = 0.0047$). For upcoming search successes, we observed the strongest ITI response in

voxels with pRFs closest to the target location, and this response became weaker as pRFs got further away ($F_{7,217} = 4.25$, $p = 0.0002$). For upcoming search failures, there was no evidence for differential coding of the target (vs. other) locations during the ITI ($F_{7,217} = 0.18$, $p = 0.98$). The difference between successes and failures was maximal in voxels whose pRFs were closest to the target location (success vs failure at angular distance of 0: $t_{31} = 3.92$, $p = 0.00045$; Fig. 4B), indicating that preparatory activity in these voxels may be driving differences in behavior. Overall, these results demonstrate that memory-based predictions lead to spatially precise preparatory representations in early visual cortex. This precise preparatory coding in turn predicts the accuracy of upcoming eye movements during visual search.

A Preparatory location coding in visual cortex



B



C

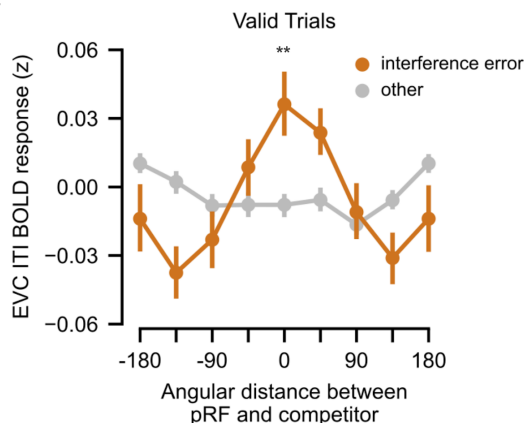


Figure 4. Preparatory target coding in early visual cortex predicts search success, whereas preparatory competitor coding predicts search failure due to interference. (A) During the inter-trial interval (ITI), participants maintained fixation while simultaneously engaging in memory-based prediction, allowing us to examine spatially organized preparatory activity in early visual cortex (EVC) during the blank delay. To do this, we isolated BOLD responses corresponding to the blank ITI of the search task, separately for voxels with population receptive fields (pRFs) that varied in distance from the target or competitor locations. pRFs for every voxel were estimated using data acquired from a separate retinotopic mapping task. **(B)** We examined valid trials and compared preparatory coding of target locations for upcoming search successes and failures. Preparatory activity was higher around the target location during ITIs immediately followed by search

successes, relative to ITIs followed by search failures (successes vs. failures at target pRFs: $t_{31} = 3.92$, $p = 0.00045$). Points and error bars represent the across-participant mean and bootstrapped SEM. **(C)** We repeated the same procedure, instead comparing preparatory coding of competitor locations for upcoming interference errors and other responses. Preparatory activity was higher around the competitor location during ITIs immediately followed by interference errors, relative to ITIs followed by other responses (interference vs. other responses at competitor pRFs: $t_{31} = 3.31$, $p = 0.0023$). Points and error bars represent the across-participant mean and bootstrapped SEM.

We next asked whether the presence of memory competition between scene pairmates (see Fig. 2D and 2E) led to preparatory coding of the competitor location and what consequences that had for behavior. We hypothesized that early visual cortex would contain representations of the competing location during the blank ITI, but that these representations would be associated with interference errors, rather than successful search. We performed the same procedure as in the prior analysis, but sorting voxels based on their distance to the competitor location and averaging separately for upcoming interference errors and other trials. Because we focused on valid trials, interference errors were searches that ended at the competitor location, despite the fact that the distortion was in the target location. Consistent with our hypothesis, location representations for upcoming interference errors were different from other trials (angular distance from competitor \times interference/other interaction: $F_{7,217} = 5.19$, $p < 0.0001$). The difference was maximal in voxels with pRFs closest to the competitor location, such that elevated ITI activity in pRFs at the competitor location was associated with upcoming interference errors (interference vs other at angular distance of 0: $t_{31} = 3.31$, $p = 0.0023$; Fig. 4C). These results demonstrate that preparatory representations in early visual cortex can also reflect *inaccurate* predictions that occur as a result of memory competition. In this case, these representations are associated with errors in attentional allocation that lead to task failure. Taken together, our findings in visual cortex show that preparatory coding predicts the successful use of memory to guide attention as well as failure caused by competition.

Hippocampal memory differentiation reduces preparatory activation of competitor locations in visual cortex

Next, we asked whether differentiation of scene pairmates in the hippocampus influenced the relative activation of target and competitor locations in visual cortex. We hypothesized that scene differentiation in the hippocampus would reduce the activation of competitor locations in visual cortex, allowing preparatory representations in this region to be more precise. To test this hypothesis, we used our pRF-based approach to re-examine preparatory target and competitor location coding in visual cortex during the ITI of valid trials, separately for scenes that were more vs. less differentiated in the hippocampus (following the procedure in Fig. 3A). We focused on scene pairs for which the target and competitor locations were 45 degrees apart (adjacent locations in our study) because they posed the most memory competition. We first visualized ITI activity in early visual cortex as a function of pRF distance from the target location, separately for 45 degree pairs that were more vs. less differentiated by the hippocampus. Consistent with our hypothesis, we observed qualitatively different activation profiles in visual cortex according to the

level of hippocampal differentiation. For scene pairs that were *less* differentiated by the hippocampus, we observed comparable preparatory activity in visual cortex pRFs that were responsive to the target location and those that were responsive to the competitor location (Fig. 5A, left). However, for scene pairs that were *more* differentiated by the hippocampus, we observed higher preparatory activity in visual cortex pRFs responsive to the target than in pRFs responsive to the competitor, resulting in a more precise representation (Fig. 5A, right).

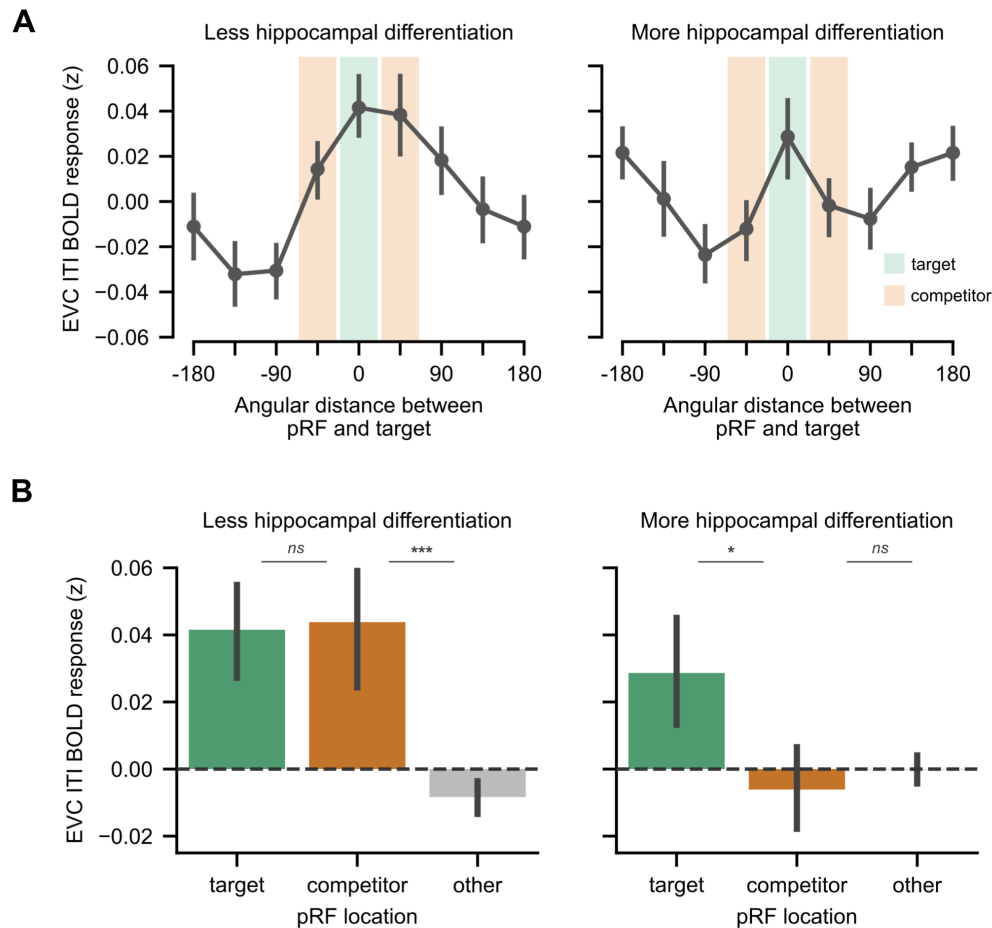


Figure 5. Hippocampal differentiation reduces preparatory activation of competitor locations in visual cortex. (A) We examined how hippocampal differentiation of similar scenes influenced preparatory visual cortical representations for the subset of scene pairs in which the target and competitor locations were adjacent (45 degrees apart). BOLD responses corresponding to the blank inter-trial interval (ITI) are plotted for early visual cortex (EVC) voxels with population receptive fields (pRFs) different distances from the target location, separately for scene pairs that were less differentiated (left) and more differentiated (right) by the hippocampus. pRFs responsive to a given scene’s target location are plotted at 0 (green shading) and pRFs responsive to the competitor location are either at +45 or -45 (orange shading) across different trials. For scene pairs that were more differentiated by the hippocampus, we observed lower competitor activation relative to target activation in visual cortex, indicating more precise preparatory representations. Preparatory representations were less precise for the scene pairs that were less differentiated by the hippocampus, as indicated by relatively higher activation of the competitor locations. Points and error bars represent the across-participant mean and bootstrapped SEM. **(B)** We quantified the data in (A) by assigning each pRF bin

the label “target”, “competitor”, or “other” location. We then examined ITI responses in visual cortex separately for each of these bins, and separately for scene pairs that were more vs. less differentiated by the hippocampus. The interaction between location bin (target/competitor/other) and hippocampal differentiation (more/less) was significant ($\chi^2 = 13.03$, $p = 0.0015$), and driven by comparable target and competitor activation in visual cortex for less differentiated pairs (beta = -0.00055, SE = 0.0078, $p = 0.94$), but lower competitor than target activation for more differentiated pairs (beta = -0.018, SE = 0.0071, $p = 0.012$). Bars and error bars represent the across-participant mean and bootstrapped SEM.

To quantify these effects, we assigned each pRF bin the label “target”, “competitor”, or “other” location for every trial and compared ITI responses in these voxel groups for more vs. less differentiated scene pairs (Fig. 5B). We used a mixed effects model to assess whether the interaction between scene pair differentiation (more vs. less) and relative BOLD activity in voxels coding for target, competitor, and other locations was statistically significant. An interactive model was a better fit to the data than an additive model ($\chi^2 = 13.03$, $p = 0.0015$), indicating that preparatory activity in visual cortex voxels coding for target, competitor, and other locations varied based on hippocampal differentiation. To clarify this interaction, we conducted follow-up comparisons separately for scene pairs that were more vs. less differentiated by the hippocampus. For less differentiated pairs, visual cortex ITI activity in competitor pRFs was comparable to target pRFs (beta = -0.00055, SE = 0.0078, $p = 0.94$) and greater than all other pRFs (beta = 0.026, SE = 0.0059, $p < 0.0001$; Fig. 5B, left). For more differentiated pairs, ITI activity in competitor pRFs was lower than in target pRFs (beta = -0.018, SE = 0.0071, $p = 0.012$) and no different from all other pRFs (beta = -0.0026, SE = 0.0055, $p = 0.63$; Fig. 5B, right). Thus, stronger differentiation of similar scenes in the hippocampus suppressed the representation of competing (vs. target) locations in visual cortex, allowing for more precise visual cortical representations prior to search onset. Interestingly, this effect was selective to the 45 degree pairs (target-competitor distance x target/competitor/other pRFs x more/less differentiated: $\chi^2_{15} = 47.7$, $p < 0.0001$; target/competitor/other pRFs x more/less differentiated for 90, 135, and 180 degree pairs: all $ps > 0.3$), consistent with work proposing that the amount of competition between memories is a driver of representational change in the brain (Ritvo et al., 2019, 2023; Wammes et al., 2022).

Discussion

Memory and perception both require selection of relevant representations in the face of competitors. Here, using a novel task, we demonstrate that mechanisms that overcome competition in memory and perception are linked via the hippocampus. First, we show that hippocampal differentiation of competing memories supports precise eye movements during memory-guided visual search. Second, we show that early visual cortex exhibits preparatory coding of target and competing search locations, with strong representations of upcoming target locations predicting search successes and strong representations of upcoming competitor locations predicting search failures due to interference. Finally, we link these findings by showing that hippocampal differentiation is associated with changes to the precision of preparatory representations in visual cortex. When hippocampal differentiation is stronger, competitor activation in visual cortex is lower, yielding more precise preparatory representations.

Our findings build on a rich literature of prior work examining the role of memory in guiding visual attention. Behavioral studies have repeatedly shown that attentional performance, such as the speed of visual search, improves with previous exposure to the search targets and/or surrounding context (Chun & Jiang, 1998; Fan & Turk-Browne, 2016; Chun & Turk-Browne, 2007; Nobre & Stokes, 2019). More recent work has illuminated the circumstances under which memories may cause interference or competition in attentional allocation and eye movements (Nickel et al., 2020; Wynn et al., 2020; Hirschstein & Aly, 2023). Complementary lesion studies (Chun & Phelps, 1999; Ryan et al., 2000; Ruiz et al., 2020) and fMRI experiments (Summerfield et al., 2006; Hannula & Ranganath, 2009; Stokes et al., 2012; Goldfarb et al., 2016; Günseli & Aly, 2020) have also begun to uncover the hippocampal and cortical mechanisms by which memories can guide attention. We were particularly inspired by prior fMRI studies showing that: 1) hippocampal activity is higher when attention is guided by memory than when it is guided by external cues (Summerfield et al., 2006; Günseli & Aly, 2020) and 2) contralateral preparatory activity in visual cortex precedes memory-guided attention (Stokes et al., 2012).

Here, we sought to extend prior work implicating the hippocampus in memory-guided attention by testing how hippocampal *computations* that differentiate memories shape the precision of attentional selection. We also sought to directly link these hippocampal computations to visual cortical representations supporting attention. We capitalized on fMRI methodological advances that allow characterization of representations in the brain, using both pattern similarity techniques and encoding models to achieve these aims. These methodological advances allowed us to go beyond prior work on memory-guided attention by showing that the way in which specific memories are represented in the hippocampus has consequences for memory-guided eye movements: when two similar memories are represented more distinctly in the hippocampus, eye movements that are guided by those memories are more precise. We also strengthened prior findings of preparatory coding in visual cortex by using sensitive pRF-based analyses (Dumoulin & Wandell, 2008; Wandell & Winawer, 2015) that allowed us to measure the activation of specific locations close to one another within a quarter visual field. Using these techniques, we show evidence for robust preparatory coding of target locations that predicts successful search behavior. Moreover, we demonstrate novel evidence for preparatory coding of competitor locations and show that hippocampal representations modulate the relative strength of targets and competitors in visual cortex. These results extend prior work showing that expectations sharpen visual cortex representations (Kok et al., 2012) by identifying hippocampal memory differentiation as a potential candidate mechanism for this increased precision. Further, our work goes beyond studies showing complementary types of prediction signals in visual cortex and hippocampus (Hindy et al., 2016; Kok & Turk-Browne, 2018) by showing how the hippocampus and visual cortex may interact to suppress competing memories in anticipation of deploying visual attention. Thus, our results validate the importance of the hippocampus in memory-guided attention and the presence of preparatory coding in visual cortex, but go beyond prior work by demonstrating new mechanistic links between hippocampal computations that resolve

competition between memories, visual cortical representations, and the precision of attentional selection.

Our work critically extends prior work on memory-guided attention to more realistic task contexts in which multiple memories compete for attention, revealing ties between how competition is resolved in memory and perception. To make this advance, we drew on recent fMRI studies examining how the hippocampus prevents interference between competing memories (Favila et al., 2016; Chanales et al., 2017; Wanja et al., 2021). These studies associated highly similar scenes with distinct outcomes and tracked how hippocampal representations of the scenes changed as memory interference was resolved. This work has found that while similar memories begin with similar hippocampal representations, these representations become differentiated with repeated competition, consistent with computational models that have proposed activity-dependent representational change in the hippocampus (Norman et al., 2006; Ritvo et al., 2019, 2023). Complementary work with MEG has shown that the hippocampus may minimize competition between overlapping memories by representing them at different phases of its ongoing theta rhythm (Kerrén et al., 2022). Here, we advance the literature on hippocampal memory differentiation in several ways. First, by associating similar scenes with distinct spatial locations, we were able to track memory competition during natural visual behavior by measuring whether eye movements were directed near target or competitor spatial locations. We found that differentiation of competing memories in the hippocampus was associated with more precise eye movements (i.e. eye movements that were closer to the target location) during memory-guided visual search. Thus, our study demonstrates that hippocampal differentiation is not just important for direct assessments of memory, but also for natural perceptual behaviors in which memory must be combined with ongoing sensory input. This finding adds to the growing literature suggesting that the separability of hippocampal representations is important for diverse cognitive functions, including navigation (Fernandez et al., 2023), control (Jiang et al., 2020), and reinforcement learning (Ballard et al., 2019). Second, by capitalizing on methods from visual neuroscience that allow for precise estimation of spatial receptive fields, we were able to link hippocampal differentiation to more precise preparatory activity in visual cortex. This goes beyond prior work on hippocampal differentiation, which has failed to demonstrate that differentiation has any consequences for cortical memory representations.

Our results raise interesting questions about the interplay between the hippocampus and cortex during memory-guided behaviors. In our task, we purposely designed a blank ITI period during which visual fixation was enforced so that we could measure spatial responses in early visual cortex in the absence of visual stimulation. Spatially-specific activity measured during this interval must have a top-down source elsewhere in the brain. For this reason, we interpret our results linking hippocampal differentiation to preparatory coding in visual cortex as reflecting a modulation of visual cortex by the hippocampus and not the other way around. It is possible, however, that during initial learning, attentional modulation of visual cortex representations contributes to hippocampal differentiation by adjusting input to the hippocampus (Amer &

Davachi, 2023). In this way, there could be bidirectional interactions between the hippocampus and visual cortex occurring at different times.

Our focus on the hippocampus as a top-down modulator is justified given strong behavioral evidence that memory is contributing to attentional behavior in our task, as well as prior work implicating the hippocampus in memory-guided attention (Chun & Turk-Browne, 2007; Aly & Turk-Browne, 2017) and showing its necessity for preparatory coding in visual cortex (Finnie et al., 2021). However, it is possible that other brain areas are also supplying top-down drive to visual cortex and/or the hippocampus. Candidate areas for such modulation include control-related regions of prefrontal and parietal cortex that are implicated in the control of visual attention (Corbetta & Shulman, 2002) and memory-guided attention (Rosen et al., 2015, 2016) and in resolving memory competition (Wimber et al., 2015; Anderson & Hulbert, 2021). One intriguing possibility is that control-related cortical regions play an important role in enabling top-down spatial attention in the face of memory competition early in learning when hippocampal memories are not well formed or too overlapping to prevent interference. However, once hippocampal memory representations are sufficiently differentiated, the need for control resources may be reduced (Kuhl et al., 2007). The influence of top-down control areas may also explain why we observed a relationship between distinct hippocampal representations and preparatory activity in visual cortex only for memories with the highest similarity. High levels of memory similarity may necessitate more influence from the hippocampus, which is thought to be uniquely suited to discriminate overlapping neural codes, while control-related regions may be able to regulate visual cortical representations in other cases. Future work can test these ideas by tracking the engagement of different neocortical systems and their interaction with the hippocampus as memories are acquired and as they are subsequently used to guide behavior.

To conclude, we show that hippocampal mechanisms for differentiating competing memories influence the precision of attentional selection and modulate preparatory activity in the visual system. Our results demonstrate linked mechanisms that overcome competition in memory and perception and argue for a broad role for memory systems in shaping adaptive perceptual behavior.

Methods

Participants

Thirty-six human participants were recruited from the Columbia University community and the surrounding area. Participants provided written informed consent prior to participating in the experiment and were compensated \$20/hr for their time. All experimental procedures were approved by the Columbia University Institutional Review Board. We excluded all data acquired from four participants from our analyses. Three participants were excluded because they withdrew from the experiment during the first experimental session due to difficulty with the task. MRI data was not acquired for these participants. One participant was excluded because of low

eye-tracking data quality from the MRI session (> 3 standard deviations below the mean number of usable trials across participants). The final sample of 32 participants consisted of 15 male individuals, 16 female individuals, and 1 non-binary individual. Participants included 11 individuals who identified as White, 9 who identified as Hispanic/Latino and White, 3 who identified as Black or African-American, 1 who identified as Hispanic/Latino and Black or African-American, 5 who identified as Asian, and 3 who identified as multiracial. Participants were 18–31 years old (median = 21) and had 12–20 years of education (median = 15.5). All participants were right-handed, had normal or corrected-to-normal visual acuity, normal color vision, and no MRI contraindications.

Stimuli

Scenes

There were 24 critical scene stimuli, comprising 12 pairs of highly similar scene images (pairmates). Each pair belonged to a distinct outdoor scene category: apple orchards, arches, barns, canyons, castles, cities, gazebos, lighthouses, ponds, roller coasters, vineyards, and waterfalls. The two scene pairmates from each category were handpicked to have high levels of perceptual similarity. We validated perceptual similarity by running the scenes through three convolutional neural network models (alexnet, vgg16, and resnet50) that approximate high-level visual cortex (Yamins et al., 2014; Eickenberg et al., 2017; Lindsay, 2020) and were pretrained to classify scenes. We used late layer activations from these models to compute scene similarity matrices of our stimulus set. Pairmate similarity distributions were higher than and non-overlapping with non-pairmate similarity distributions in all models, validating our pairmate similarity structure. Beyond these critical scenes, an additional 56 outdoor scenes were used as novel images in the fMRI task only. These scenes were hand selected to have low perceptual similarity with the scene pair stimuli and with each other. Throughout the experiment, scenes were displayed in the center of the screen and were sized to be 15 x 15 degrees of visual angle. Participants never saw any two scenes presented simultaneously for comparison.

Locations

Eight isoeccentric (eccentricity = 3.3 degrees) spatial locations were evenly sampled across polar angles ($\theta = 22.5, 67.5, 112.5, 157.5, 202.5, 247.5, 292.5, \text{ or } 337.5$ degrees). During learning, locations were always visualized as a white circle with a green outline centered at one of these locations and with a radius of 0.75 degrees of visual angle. Participants never saw the eight locations highlighted simultaneously.

Scene Distortions

Spatially localized distortions were created in the scene images by vertically displacing a local patch of pixels according to a sinusoidal function. The distortion was smoothly modulated by a fixed 2D Gaussian function so that the distortion was strongest at the center and faded gradually outwards. Perceptually, this resulted in a small circular patch of the image looking “wavy” with no hard boundary between the distorted patch and the rest of the image. For each of the 24 critical

scene stimuli and each of the 56 novel scene stimuli, we created eight different distorted images. Each version of an image contained a single distorted location centered at one of the eight isoecentric spatial locations used in the competitive learning task. To create each distorted image, we initially used a sinusoid with a fixed spatial frequency, a fixed amplitude, and a randomly selected phase, centered at the distortion location and smoothed with a 2D Gaussian. Then, to equate the difficulty of identifying distortions across different images and across different locations within an image, we ran a separate online experiment. Online participants viewed the initial images one at a time for 3 s each and were instructed to click on the distortion as quickly as possible. Based on participants' ability to detect the distortions, we separately adjusted the amplitude of the sinusoid (distortion strength) up or down for each image and location, targeting an accuracy of 50% for each image and location across participants. We did this iteratively across four rounds of data collection, resulting in final distortion strengths that were tailored to each location within each image. We purposely chose a relatively modest accuracy threshold for this norming study to ensure that detecting the distortions was difficult enough to encourage participants to use memory to guide their attention in the main search task.

Experimental Design and Procedure

The experiment consisted of two sessions, which occurred on consecutive days. In the first session (behavior only), participants performed a competitive learning task during which they acquired competing scene-location associations. The following day, participants performed a memory-guided visual search task while being scanned with fMRI. This task required participants to use the scene-location associations they acquired in the first session to improve their search performance. Participants also performed a population receptive field mapping task (see *Session 2: Retinotopic Mapping Task (fMRI)*) and localizer task (not analyzed here) while being scanned. All tasks were implemented in PsychoPy. Design and procedure details for each session and task are described below.

Session 1: Competitive Learning Task (Behavioral)

The goal of the first session was for participants to learn competing scene-location associations. There were three types of blocks in this session: scene exposure, study, and test. Participants' eye movements were collected continuously in all three block types.

Scene Exposure. Participants began the session with two blocks of scene exposure. They were instructed that this was an opportunity to become familiar with the scenes before learning the scene-location associations, and that some scenes would be similar to each other. In each scene exposure block, participants were presented with each of the 24 critical scenes one time. Scenes were presented in a random order with the constraint that pairmates not be presented back to back. Each scene was presented on a gray background for 2 s. Participants' eye movements were unrestricted during scene presentation. A 2 s central fixation interval occurred in between trials. Fixation on the central dot during the intertrial interval was enforced with a beep in response to fixation breaks.

Scene-Location Associations. After completing the scene exposure blocks, participants acquired 24 scene-location associations. Critically, some of these memories competed with each other because of the pairmate structure of the scenes. Scene-location associations were determined according to the following procedure. Each of the 24 critical scenes was assigned to predict one of the eight spatial locations. This was done randomly for each participant such that: 1) pairmate scenes were never associated with the same location; 2) the distance between two pairmates' associated locations (45, 90, 135, or 180 degrees) was balanced; 3) all eight locations were sampled evenly. We refer to the location associated with a scene as that scene's target location and the location associated with the pairmate scene as the competitor location.

Study and Test Blocks. Participants acquired the scene-location associations through study and test blocks. During study blocks, participants were presented with scene-location associations one time each and were instructed to explicitly encode the associations to the best of their ability. At the start of each study trial, a scene was presented on a gray background for 2 s, followed by that scene's associated location for 2 s. The location (see *Methods/Stimuli/Locations*) was overlaid on a dark gray box the same size as the scene. Participants' eye movements were unrestricted during scene and location presentation. A 2 s enforced central fixation interval occurred in between study trials. Study trial order was randomized within a block with the constraint that scene pairmates not be presented in consecutive trials. During test blocks, participants were tested on their memory for the scene-location associations one time each. They were instructed to recall the associations as accurately as possible and to guess if necessary. At the start of each test trial, a scene cue was presented on a gray background for 2 s, followed by a 2 s enforced central fixation interval. The response period began immediately after this with the onset of a blank dark gray box the same size as the scene. Participants were instructed to make a memory-guided saccade to the cued scene's associated location during this period and to hold their gaze at the remembered location. The response period lasted 2 s and the participant's average eye position in the final 200 ms of the response period (excluding blinks) was recorded as their response. Angular error was computed as the angular distance between this response and the center of the correct location. Immediately following the response period and regardless of the participant's response, the correct location was presented for 1 s as feedback. Participants' eye movements were unrestricted during scene presentation and location feedback. A 2 s enforced central fixation interval occurred in between test trials. Test trial order was randomized within a block with the constraint that scene pairmates not be presented in consecutive trials. At the end of each test block, participants were shown a block feedback screen that reported their average angular error as well as the percentage of trials for which their response was closer to the target location than to the competitor location.

Block Order and Performance Evaluation. To ease the difficulty of the task, participants first performed three consecutive study-test rounds on 12 scene-location associations (6 scene pairs). They then repeated the process for the remaining 12 scene-location associations. After performing the second set of three study-test rounds, participants performed two test blocks in

which they were tested on all 24 scene-location associations. If a participant achieved an average angular error of 20 degrees or less across these two blocks, the learning task was terminated. If a participant did not meet this threshold, they continued performing test blocks until the average of their last two blocks met this threshold or until the end of the 1.5 hour session was reached. We targeted these extra test blocks toward poorly learned pairs by dropping well-learned pairs from the blocks. Well-learned pairs were pairs for which the participant responded within 20 degrees of angular error to both pairmates on two consecutive blocks.

Session 1: Distortion and Search Practice (behavioral)

At the end of Session 1, participants did two short practice tasks that prepared them for the scanned search task in the next session. Participants were told that their task the next day would involve searching for distortions hidden in scenes. They were then given a short task designed to introduce them to what these distortions looked like. Participants viewed 30 example images with representative distortions, one at a time. The task was self-paced, allowing participants to search for each distortion for as long as they wanted before choosing to reveal the location of the distortion. None of the distorted images in this task appeared in the next session. Then, participants were instructed on the search task (see next section) and practiced a modified version of it with the 24 critical scenes while their eye movements were recorded. In this modified version, participants were given longer to search for the distortions (2.75 s vs. 1.25 s in the fMRI task) and all trials were valid.

Session 2: Memory Refresher and Search Practice (behavioral)

At the start of session 2, immediately before entering the scanner, participants did two short practice tasks to prepare them for the scanned search task. First, participants were re-tested on the scene-location associations that they learned the previous day. They then practiced the version of the search task that they would perform in the scanner. Both of these tasks used an eye-tracking setup equivalent to the one used in session 1, but located in the same building as the MRI facility. The exact number of practice blocks/trials was based on participant performance and comfort with the task.

Session 2: Memory-guided Visual Search Task (fMRI)

The goal of the second session was for participants to use their memories of the scene-location associations to guide performance in a novel visual search task. Participants completed the search task while being scanned with functional MRI (see *MRI Acquisition*) and while their eye movements were recorded continuously (see *Eye Tracking Data Acquisition*).

Task Design. The purpose of the task was to measure participants' ability to use competing memories to guide online attentional behavior. To encourage reliance on memory, we designed a visual search task that was challenging to perform under the chosen task parameters (high search difficulty and short stimulus presentation). On each trial of this task, participants had 1.25 s to search a scene image for a small local distortion (see *Stimuli/Scene Distortions*). Under these

conditions and based on our distortion norming experiment and other preliminary pilot data, participants were expected to locate the distortion on less than half of trials. Critically, we embedded structure in the task that allowed participants to improve their search performance if they could recall the scene-location associations they learned the previous day. Specifically, consecutive trials were linked such that each scene was both a search array (i.e. it contained one distortion) *and* a cue for the subsequent trial. If participants saw one of the 24 critical scene stimuli from session 1 in the trial sequence, that meant that the scene's associated target location was the most likely location of the distortion on the *next* trial. This manipulation encouraged participants to recall the prior scene's target location during the intertrial interval to predict the distortion location on the upcoming trial. There were three conditions of interest: validly cued trials, invalidly cued trials, and no-prediction trials. On validly cued trials, which were 75% of all trials, the distortion was placed in the previous scene's target location. On invalidly cued trials, which were 12.5% of all trials, the distortion was placed in the location associated with the previous scene's competitor (i.e., the target location of the previous scene's pairmate). On no-prediction trials, which were 12.5% of all trials, the distortion was placed randomly in one of the eight possible distortion locations. These trials were always preceded by one of the trial-unique novel scenes, which had no associated target location (see *Stimuli/Scenes*). Trial orders were constructed such that the critical manipulation between scene identity and the next trial's distortion location was the only exploitable structure. Scenes only predicted distortions on the *upcoming* trial; there was no link between scene identity and the location of the distortion on that particular trial. With the exception that scene pairmates were never presented in back-to-back trials, upcoming scene identity was not predictable. All of the 24 critical scene stimuli were equally likely to be validly cued and (within a tolerance) to be valid cues. All eight locations were equally likely to be the learned target location relevant for the next trial. Distortions occurred at all eight locations with approximately equal probability.

Task Parameters and Procedure. Participants performed eight consecutive runs of the search task in the MRI scanner with short breaks in between each run. On each trial of the task, a scene was presented on a gray background for 1.25 s. Every scene contained one local distortion, which occurred at one of eight isoeccentric locations (see *Stimuli/Scene Distortions*). The onset of scene presentation cued participants to begin their search. Participants were instructed to move their eyes to find each scene's distortion as quickly as possible and to fixate the distortion when they found it. Participants' entire eye movement trajectory was recorded, but for the purpose of generating feedback, the final 200 ms of their eye position was recorded and averaged excluding blinks. If this position was within 20 degrees of angular error from the center of the distortion location, the trial was considered correct. At the offset of scene presentation, an intertrial fixation interval began. This interval was randomly selected to be 4.75 s, 6.25 s, or 7.75 s with equal probability. For the first .75 s of the interval, the central fixation dot was green (if the previous trial was correct) or red (if the previous trial was incorrect), and for the rest of the interval it was white. Participants were explicitly instructed of the contingency between consecutive trials and were told to aim for 70% accuracy by relying on their memories to predict the location of upcoming distortions. They were also instructed to maintain fixation on the central fixation dot

while preparing for the next trial. At the end of each run, participants were shown a feedback screen that reported their average accuracy for that run. Each run took a little over seven minutes to complete and contained 56 trials. The first trial in each run was discarded from behavioral analyses since it was not cued. Among the 55 cued trials per run, there were 41 validly cued trials, 7 invalidly cued trials, and 7 no-prediction trials. The 55 cued trials always consisted of two presentations each of the 24 critical scenes and one presentation each of 7 trial-unique novel scenes. Across all eight runs of the task, each of the 24 critical scenes was presented 16 times; 12 of these presentations were validly cued trials, 2 were invalidly cued trials, and 2 were no-prediction trials.

Session 2: Retinotopic Mapping Task (fMRI)

After completing the search task, each participant completed four identical retinotopic mapping runs. Stimuli and task parameters for the retinotopic mapping session were based on those reported previously (Benson & Winawer, 2018; Himmelberg et al., 2021; Favila et al., 2022), but a smaller portion of the visual field was mapped. During each functional run, bar apertures on a uniform gray background swept across the central 15 degrees of the participant's visual field (a circular aperture with a radius of 7.5 degrees visual angle). Each sweep began at one of eight equally spaced positions around the edge of the circular aperture, with the bar oriented perpendicularly to the direction of the sweep. During horizontal and vertical sweeps, the bar moved from one side of the aperture to the other at a constant rate. During diagonal sweeps, the bar moved at a constant rate until it reached the midpoint of the aperture; it then disappeared and was followed by a blank period that allowed for measurement of baseline neural activity. The bar position was incrementally updated every 1 s, such that a full-field sweep across the entire aperture took 24 s. Half-field sweeps took 12 s and subsequent blank periods took 12 s (24 s total). One functional run contained 8 back-to-back sweeps, taking 192 s in total. Bar apertures were a constant width and contained a grayscale pink noise background with randomly placed faces, scenes, objects, and words at a variety of sizes. Noise background and stimuli were updated at a frequency of 3Hz. Each run of the task had identical timing, bar positions, sweep order, and stimuli. Participants were instructed to maintain fixation on a central dot and to use a button box to report whenever the dot changed color from blue to green or green to blue. Color changes occurred 24 times per run, and their timing was randomized for each participant and run.

Eye Tracking Data Acquisition

Eye tracking data were collected using an Eyelink 1000 Plus infrared video-based system by SR Research. For all sessions, the camera tracked the participant's right eye at 1000 Hz in a head-stabilized position. During session 1, participants were stabilized in a chinrest and the camera was positioned below the task display. During session 2, participants were stabilized in the head coil and an MRI-compatible long-range enabled Eyelink 1000 Plus system was positioned outside the scanner bore and beneath the MRI display such that the participant's eye could be tracked through the head coil-mounted mirror. In both sessions we calibrated the eye

tracker using a 9 point calibration scheme at the start of each task block or scanner run or as needed.

Eye Tracking Preprocessing and Analysis

Raw gaze data from session 1 and session 2 were preprocessed to identify saccades during task periods of interest. For session 1, we extracted gaze data from the response period of test trials and converted the gaze coordinates from pixels into degrees of visual angle. We removed the 200 ms prior to blinks and the 200 ms after blinks to remove artifacts. We used smoothed gaze data to define saccades as eye movements with a velocity of at least 30 deg/s and an amplitude of at least 0.25 deg (Li et al., 2021). Fixations were defined to be periods of stable gaze position occurring between saccades, excluding blinks. We corrected saccade trajectories based on the longest fixation of the pretrial central fixation period to account for drift. For our analyses, we dropped all saccades that landed within 1 degree of central fixation; of the remaining saccades, we analyzed the end points of the first and last saccade with respect to that trial's target and competitor locations. For session 2, we performed the same procedure, but on gaze data from the scene presentation period of search trials.

MRI Acquisition

All MRI data were acquired on a 3T Siemens Magnetom Prisma system located at Columbia University's Zuckerman Mind Brain Behavior Institute. Functional images were acquired using a Siemens 64-channel head/neck coil and a multiband EPI sequence (repetition time = 1.5s, echo time = 30ms, flip angle = 65°, acceleration factor = 3, voxel size = 2 x 2 x 2mm, phase encoding direction = posterior to anterior). Sixty-nine oblique axial slices (14° transverse to coronal) were collected in an interleaved order. Each participant also underwent a T1-weighted anatomical scan (resolution = 1 x 1 x 1mm) using a magnetization-prepared rapid acquisition gradient-echo (MPRAGE) sequence. Double-echo gradient echo images were acquired to estimate the susceptibility-induced distortion present in the functional EPIs. In two participants, an opposite phase encoded field map sequence (anterior to posterior and posterior to anterior) was collected instead.

MRI Preprocessing

Results included in this manuscript come from preprocessing performed using fMRIPrep 21.0.0 (Esteban, Blair, et al., 2019; Esteban, Markiewicz, et al., 2019; RRID:SCR_016216), which is based on Nipype 1.6.1 (Gorgolewski et al., 2011; RRID:SCR_002502).

Preprocessing of B_0 Inhomogeneity Mappings

A B_0 nonuniformity map (or fieldmap) was estimated from the phase-drift map(s) measure with two consecutive GRE (gradient-recalled echo) acquisitions. The corresponding phase-map(s) were phase-unwrapped with prelude (FSL 6.0.5.1:57b01774).

Anatomical Data Preprocessing

The T1-weighted (T1w) image was corrected for intensity non-uniformity (INU) with N4BiasFieldCorrection (Tustison et al., 2010), distributed with ANTs 2.3.3 (Avants et al., 2008; RRID:SCR_004757), and used as T1w-reference throughout the workflow. The T1w-reference was then skull-stripped with a Nipype implementation of the antsBrainExtraction.sh workflow (from ANTs), using OASIS30ANTs as target template. Brain tissue segmentation of cerebrospinal fluid (CSF), white-matter (WM) and gray-matter (GM) was performed on the brain-extracted T1w using fast (FSL 6.0.5.1:57b01774, RRID:SCR_002823, Zhang et al., 2001). Brain surfaces were reconstructed using recon-all (FreeSurfer 6.0.1, RRID:SCR_001847, Dale et al., 1999), and the brain mask estimated previously was refined with a custom variation of the method to reconcile ANTs-derived and FreeSurfer-derived segmentations of the cortical gray-matter of Mindboggle (RRID:SCR_002438, Klein et al., 2017). Volume-based spatial normalization to one standard space (MNI152NLin2009cAsym) was performed through nonlinear registration with antsRegistration (ANTs 2.3.3), using brain-extracted versions of both T1w reference and the T1w template. The following template was selected for spatial normalization: ICBM 152 Nonlinear Asymmetrical template version 2009c (Fonov et al., 2009, RRID:SCR_008796; TemplateFlow ID: MNI152NLin2009cAsym).

Functional Data Preprocessing

For each of the BOLD runs per participant, the following preprocessing was performed. First, a reference volume and its skull-stripped version were generated using a custom methodology of fMRIPrep. Head-motion parameters with respect to the BOLD reference (transformation matrices, and six corresponding rotation and translation parameters) are estimated before any spatiotemporal filtering using mcflirt (FSL 6.0.5.1:57b01774, Jenkinson et al., 2002). The estimated fieldmap was then aligned with rigid-registration to the target EPI (echo-planar imaging) reference run. The field coefficients were mapped on to the reference EPI using the transform. BOLD runs were slice-time corrected to 0s for retinotopic mapping runs and 0.708s for memory-guided search runs using 3dTshift from AFNI (Cox & Hyde, 1997, RRID:SCR_005927). The BOLD reference was then co-registered to the T1w reference using bbregister (FreeSurfer) which implements boundary-based registration (Greve & Fischl, 2009). Co-registration was configured with six degrees of freedom.

Several confounding time series were calculated based on the preprocessed BOLD: framewise displacement (FD), DVARS and three region-wise global signals. FD was computed using two formulations following Power (absolute sum of relative motions, Power et al., 2014) and Jenkinson (relative root mean square displacement between affines, Jenkinson et al., 2002). FD and DVARS are calculated for each functional run, both using their implementations in Nipype (following the definitions by Power et al., 2014). The three global signals are extracted within the CSF, the WM, and the whole-brain masks. Additionally, a set of physiological regressors were extracted to allow for component-based noise correction (CompCor, Behzadi et al., 2007). Principal components are estimated after high-pass filtering the preprocessed BOLD time series (using a discrete cosine

filter with 128s cut-off) for the two CompCor variants: temporal (tCompCor) and anatomical (aCompCor). tCompCor components are then calculated from the top 2% variable voxels within the brain mask. For aCompCor, three probabilistic masks (CSF, WM and combined CSF+WM) are generated in anatomical space. The implementation differs from that of Behzadi et al. in that instead of eroding the masks by 2 pixels on BOLD space, the aCompCor masks are subtracted a mask of pixels that likely contain a volume fraction of GM. This mask is obtained by dilating a GM mask extracted from the FreeSurfer's aseg segmentation, and it ensures components are not extracted from voxels containing a minimal fraction of GM. Finally, these masks are resampled into BOLD space and binarized by thresholding at 0.99 (as in the original implementation). Components are also calculated separately within the WM and CSF masks. For each CompCor decomposition, the k components with the largest singular values are retained, such that the retained components' time series are sufficient to explain 50 percent of variance across the nuisance mask (CSF, WM, combined, or temporal). The remaining components are dropped from consideration. The head-motion estimates calculated in the correction step were also placed within the corresponding confounds file. The confound time series derived from head motion estimates and global signals were expanded with the inclusion of temporal derivatives and quadratic terms for each (Satterthwaite et al., 2013). Frames that exceeded a threshold of 0.5 mm FD or 1.5 standardized DVARS were annotated as motion outliers.

The BOLD time series were resampled into standard space, generating a preprocessed BOLD run in MNI152Nlin2009cAsym space. The BOLD time series were resampled onto the following surfaces (FreeSurfer reconstruction nomenclature): fsaverage, fsnative. All resamplings can be performed with a single interpolation step by composing all the pertinent transformations (i.e. head-motion transform matrices, susceptibility distortion correction when available, and co-registrations to anatomical and output spaces). Gridded (volumetric) resamplings were performed using antsApplyTransforms (ANTs), configured with Lanczos interpolation to minimize the smoothing effects of other kernels (Lanczos, 1964). Non-gridded (surface) resamplings were performed using mri_vol2surf (FreeSurfer).

Many internal operations of fMRIPrep use Nilearn 0.8.1 (Abraham et al., 2014, RRID:SCR_001362), mostly within the functional processing workflow. Note that the analyses presented in this paper only make use of preprocessed BOLD data in native T1w and fsnative spaces.

pRF Model Fitting

pRF model fitting was conducted using vistasoft using an approach described by Dumoulin & Wandell (2008). We took the preprocessed BOLD time series from the retinotopic mapping task in native surface space and upsampled them to a temporal resolution of 1.0s to match the rate at which the bar stimulus moved. We then averaged them across runs. Using this average time series, we estimated the best fitting pRF for each vertex. Each pRF was modeled as a circular 2D Gaussian, parameterized by values x , y , and σ . The x and y parameters specify the center position of the 2D Gaussian in the visual field. These parameters can be re-expressed in polar coordinates: r (eccentricity), θ (polar angle). The σ parameter, the standard deviation of the 2D

Gaussian, specifies the size of the receptive field. Stimulus images from the retinotopic mapping task (*Methods/Experimental Design and Procedure/Session 2: Retinotopic Mapping Task*) were converted to contrast apertures. Candidate pRFs were multiplied pointwise by the stimulus apertures to yield a predicted time course of activation by the stimulus, which was then convolved with a hemodynamic response function to predict the BOLD response in each vertex. Using an iterative coarse-to-fine fitting approach, we estimated the x , y , and σ parameters for each vertex that, when applied to the drifting bar stimulus, minimized the difference between the observed and predicted BOLD time series.

Regions of Interest

The hippocampus was defined bilaterally in each participant's native anatomical space using Freesurfer. Visual cortex regions of interest were defined by visualizing the pRF parameters on each participant's native cortical surface and hand-drawing boundaries between visual field maps. For each of V1, V2, and V3, we drew boundaries at polar angle reversals, following established practice (Dougherty et al., 2003; Wandell et al., 2007). We combined bilateral V1, V2, and V3 surface masks into a single early visual cortex (EVC) ROI. This ROI was projected to native T1 space to create a volumetric EVC ROI for some analyses.

Pattern Similarity Analyses

To estimate the pattern of activity evoked by similar scenes, we conducted a voxelwise GLM analysis of each participant's preprocessed time series data from the search task in native T1 space. Each model contained a regressor of interest for each stimulus in the experiment (24 critical scenes [12 pairs of similar scenes] and 56 novel scenes). Events within these regressors were constructed as boxcars with a duration of 1.25s (scene presentation duration), convolved with a double-gamma hemodynamic response function. Six realignment parameters and cosine drift parameters were included as nuisance regressors to control for motion confounds and signal drift. No spatial smoothing was performed. We included all eight runs of the memory-guided search task in each GLM, representing 16 presentations of each of the 24 critical scenes, with the exception of one participant. One run was excluded from this participant because >10% of TRs had a framewise displacement of > 1mm. First level models were estimated using nilearn (Abraham et al., 2014) and contrasts for each of the 24 critical scenes versus baseline were computed. While regressors for the novel scenes were included in these models, these parameter estimates were not analyzed further. This procedure yielded t-maps representing the activation elicited by viewing each of the 24 critical scenes (12 pairs of similar scenes) for each participant.

To compute scene pair pattern similarity, we calculated the Fisher z-transformed Pearson correlation between the t-maps for all unique pairwise combinations of the 24 scenes. For each stimulus category (e.g., arches), we averaged all the correlations between nonpairmate scenes that included a scene from that category (e.g., arch 1 and barn 1; arch 2 and barn 1, etc). We subtracted this value from the correlation of the two pairmate scenes from that category (e.g.,

arch 1 and arch 2). Using this metric, lower values indicate that scene pairmates are represented more distinctly compared to other scenes and higher values indicate that scene pairmates are represented more similarly. To assess the overall tendency of a brain region to differentiate similar scenes, we conducted these analyses separately within brain regions of interest (hippocampus and EVC) and averaged the scene pair pattern similarity values across the 12 scene pairs to produce one value per participant. To assess the relationship between hippocampal differentiation and other variables of interest, we sorted the scene pairs by their scene pair pattern similarity value in the hippocampus and divided them into more and less differentiated halves.

Visual Cortex Preparatory Responses

We examined preparatory BOLD responses during the inter-trial interval (ITI) period of the search task by first removing the responses evoked by the preceding scene presentation and then segregating residual ITI responses according to their visual field position. To remove the visually-evoked responses, we conducted a voxelwise GLM analysis of each participant's preprocessed time series data from the search task in native surface space. (Note that we use the term "voxel" in the Results for convenience to readers, but pRF analyses are done on vertices in surface space rather than voxels in volume space). Each model contained two regressors of interest: one for presentations of the 24 critical scenes (12 pairs of similar scenes) and one for presentations of the novel scenes. These regressors and nuisance regressors were constructed using the same procedure as described in the *Pattern Similarity Analyses* subsection above, and the models were estimated using the same data inclusion criteria. We took the residual time series after estimating this model and z-scored each vertex across time and then each time point across vertices.

Using these residual time series, we isolated the time points corresponding to the first 3 TRs of the blank ITI of the search task after accounting for hemodynamic lag. This corresponded to TRs 4, 5, and 6 from scene onset. We chose 3 TRs because all trials had at minimum 3 TRs for the ITI; this allowed us to keep the amount of data constant across trials that varied in ITI duration. We averaged the residual time series across these TRs for each trial, generating one ITI BOLD response value per vertex per trial. We considered only valid trials for further analyses. To understand how these ITI responses corresponded to visual space, we organized these responses according to the values of the parameter estimates derived from the pRF model. We first selected the subset of EVC vertices that were potentially responsive to the 8 potential target locations in our experiment. We included vertices whose pRFs met 3 criteria: (1) they had eccentricity values between 0.5 and 10 degrees, indicating they were responsive to the display screen excluding central fixation; (2) the center of the 2D Gaussian was within 2σ of the circle along which target locations were aligned, indicating they were additionally responsive to target and competitor locations; and (3) their pRF model R^2 was at least 0.1, indicating they exhibited spatial selectivity. We then binned these vertices into 8 bins according to the polar angle distance between their pRF and the target memory location on the upcoming trial. We z-scored the

responses again to ensure that the average response across all bins was zero and then took the median ITI response within a bin before averaging across participants. This procedure produced a spatial response function that indicates how strong the ITI response was in vertices coding for the upcoming target location and how quickly this response falls off over space. Analyses examining competitor location responses during the ITI followed the same procedure but binned vertices according to their distance from the competitor location.

Statistics

We evaluated the statistical reliability of our behavioral, pattern similarity, and visual cortex preparatory results using paired t-tests, repeated measures ANOVAs, and Pearson correlations. Reported p-values are two-tailed and evaluated at $\alpha = 0.05$. For our analyses linking hippocampal pattern differentiation and visual cortex preparatory responses, we used mixed effects models implemented in the lme4 package for R in order to handle missing data. We evaluated the strength of interactions by performing likelihood ratio tests on nested additive models. Parameter estimates, standard errors, and p-values for individual predictors are also reported when relevant. All models included random intercepts per participant. We excluded random slopes from our models to ensure that models converged and fits were non-singular.

References

- Abraham, A., Pedregosa, F., Eickenberg, M., Gervais, P., Mueller, A., Kossaifi, J., Gramfort, A., Thirion, B., & Varoquaux, G. (2014). Machine learning for neuroimaging with scikit-learn. *Frontiers in Neuroinformatics*, *8*.
<https://www.frontiersin.org/articles/10.3389/fninf.2014.00014>
- Aly, M., & Turk-Browne, N. B. (2016). Attention Stabilizes Representations in the Human Hippocampus. *Cerebral Cortex*, *26*(2), 783–796. <https://doi.org/10.1093/cercor/bhv041>
- Aly, M., & Turk-Browne, N. B. (2017). How Hippocampal Memory Shapes, and Is Shaped by, Attention. In D. E. Hannula & M. C. Duff (Eds.), *The Hippocampus from Cells to Systems* (pp. 369–403). Springer International Publishing.
https://doi.org/10.1007/978-3-319-50406-3_12
- Amer, T., & Davachi, L. (2023). Extra-hippocampal contributions to pattern separation. *eLife*, *12*, e82250. <https://doi.org/10.7554/eLife.82250>
- Anderson, M. C., & Hulbert, J. C. (2021). Active Forgetting: Adaptation of Memory by Prefrontal Control. *Annual Review of Psychology*, *72*, 1–36.
<https://doi.org/10.1146/annurev-psych-072720-094140>
- Avants, B. B., Epstein, C. L., Grossman, M., & Gee, J. C. (2008). Symmetric diffeomorphic image registration with cross-correlation: Evaluating automated labeling of elderly and neurodegenerative brain. *Medical Image Analysis*, *12*(1), 26–41.
<https://doi.org/10.1016/j.media.2007.06.004>
- Ballard, I. C., Wagner, A. D., & McClure, S. M. (2019). Hippocampal pattern separation supports reinforcement learning. *Nature Communications*, *10*, 1073.
<https://doi.org/10.1038/s41467-019-08998-1>
- Behzadi, Y., Restom, K., Liau, J., & Liu, T. T. (2007). A component based noise correction method (CompCor) for BOLD and perfusion based fMRI. *NeuroImage*, *37*(1), 90–101.
<https://doi.org/10.1016/j.neuroimage.2007.04.042>
- Benson, N. C., & Winawer, J. (2018). Bayesian analysis of retinotopic maps. *eLife*, *7*, 0–45.
<https://doi.org/10.7554/eLife.40224>
- Breedlove, J. L., St-Yves, G., Oلمان, C. A., & Naselaris, T. (2020). Generative Feedback Explains Distinct Brain Activity Codes for Seen and Mental Images. *Current Biology*, *30*(12), 2211–2224.e6. <https://doi.org/10.1016/j.cub.2020.04.014>
- Carrasco, M. (2011). Visual attention: The past 25 years. *Vision Research*, *51*(13), 1484–1525.
<https://doi.org/10.1016/j.visres.2011.04.012>
- Chanales, A. J. H., Oza, A., Favila, S. E., & Kuhl, B. A. (2017). Overlap among spatial memories triggers divergence of hippocampal representations. *Current Biology*, *27*(15), 2307–2317.e5. <https://doi.org/10.1101/099226>
- Chun, M. M., & Jiang, Y. (1998). Contextual cueing: Implicit learning and memory of visual context guides spatial attention. *Cognitive Psychology*, *36*(1), 28–71.
<https://doi.org/10.1006/cogp.1998.0681>
- Chun, M. M., & Phelps, E. A. (1999). Memory deficits for implicit contextual information in amnesic subjects with hippocampal damage. *Nature Neuroscience*, *2*(9), 844–847.

- <https://doi.org/10.1038/12222>
- Chun, M. M., & Turk-Browne, N. B. (2007). Interactions between attention and memory. *Current Opinion in Neurobiology*, *17*(2), 177–184. <https://doi.org/10.1016/j.conb.2007.03.005>
- Corbetta, M., & Shulman, G. L. (2002). Control of Goal-Directed and Stimulus-Driven Attention in the Brain. *Nature Reviews Neuroscience*, *3*(3), 215–229. <https://doi.org/10.1038/nrn755>
- Córdova, N. I., Turk-Browne, N. B., & Aly, M. (2019). Focusing on what matters: Modulation of the human hippocampus by relational attention. *Hippocampus*, *29*(11), 1025–1037. <https://doi.org/10.1002/hipo.23082>
- Cox, R. W., & Hyde, J. S. (1997). Software tools for analysis and visualization of fMRI data. *NMR in Biomedicine*, *10*(4–5), 171–178. [https://doi.org/10.1002/\(SICI\)1099-1492\(199706/08\)10:4/5<171::AID-NBM453>3.0.CO;2-L](https://doi.org/10.1002/(SICI)1099-1492(199706/08)10:4/5<171::AID-NBM453>3.0.CO;2-L)
- Dale, A. M., Fischl, B., & Sereno, M. I. (1999). Cortical surface-based analysis. I. Segmentation and surface reconstruction. *NeuroImage*, *9*(2), 179–194. <https://doi.org/10.1006/nimg.1998.0395>
- Desimone, R., & Duncan, J. (1995). Neural Mechanisms of Selective Visual Attention. *Annual Review of Neuroscience*, *18*, 193–222. <https://doi.org/10.1146/annurev.ne.18.030195.001205>.
- Dougherty, R. F., Koch, V. M., Brewer, A. A., Fischer, B., Modersitzki, J., & Wandell, B. A. (2003). Visual field representations and locations of visual areas v1/2/3 in human visual cortex. *Journal of Vision*, *3*(10), 586–598. <https://doi.org/10.1167/3.10.1>
- Dumoulin, S. O., & Wandell, B. A. (2008). Population receptive field estimates in human visual cortex. *NeuroImage*, *39*(2), 647–660. <https://doi.org/10.1016/j.neuroimage.2007.09.034>
- Eickenberg, M., Gramfort, A., Varoquaux, G., & Thirion, B. (2017). Seeing it all: Convolutional network layers map the function of the human visual system. *NeuroImage*, *152*, 184–194. <https://doi.org/10.1016/j.neuroimage.2016.10.001>
- Esteban, O., Blair, R. W., Nielson, D. M., Varada, J. C., Marrett, S., Thomas, A. G., Poldrack, R. A., & Gorgolewski, K. J. (2019). Crowdsourced MRI quality metrics and expert quality annotations for training of humans and machines. *Scientific Data*, *6*, 30. <https://doi.org/10.1038/s41597-019-0035-4>
- Esteban, O., Markiewicz, C. J., Blair, R. W., Moodie, C. A., Isik, A. I., Erramuzpe, A., Kent, J. D., Goncalves, M., DuPre, E., Snyder, M., Oya, H., Ghosh, S. S., Wright, J., Durnez, J., Poldrack, R. A., & Gorgolewski, K. J. (2019). fMRIPrep: A robust preprocessing pipeline for functional MRI. *Nature Methods*, *16*(1), 111–116. <https://doi.org/10.1038/s41592-018-0235-4>
- Fan, J. E., & Turk-Browne, N. B. (2016). Incidental Biasing of Attention From Visual Long-Term Memory. *Journal of Experimental Psychology: Learning, Memory, and Cognition*, *42*(6), 970–977. <https://doi.org/10.1037/xlm0000209>
- Favila, S. E., Chanales, A. J. H., & Kuhl, B. A. (2016). Experience-dependent hippocampal pattern differentiation prevents interference during subsequent learning. *Nature Communications*, *6*, 11066. <https://doi.org/10.1038/ncomms11066>
- Favila, S. E., Kuhl, B. A., & Winawer, J. (2022). Perception and memory have distinct spatial tuning properties in human visual cortex. *Nature Communications*, *13*, 5864. <https://doi.org/10.1038/s41467-022-33161-8>
- Fernandez, C., Jiang, J., Wang, S.-F., Choi, H. L., & Wagner, A. D. (2023). Representational

- integration and differentiation in the human hippocampus following goal-directed navigation. *eLife*, *12*, e80281. <https://doi.org/10.7554/eLife.80281>
- Finnie, P. S. B., Komorowski, R. W., & Bear, M. F. (2021). The spatiotemporal organization of experience dictates hippocampal involvement in primary visual cortical plasticity. *Current Biology*, *31*(18), 3996-4008.e6. <https://doi.org/10.1016/j.cub.2021.06.079>
- Fonov, V., Evans, A., McKinstry, R., Almlí, C., & Collins, D. (2009). Unbiased nonlinear average age-appropriate brain templates from birth to adulthood. *NeuroImage*, *47*, S102. [https://doi.org/10.1016/S1053-8119\(09\)70884-5](https://doi.org/10.1016/S1053-8119(09)70884-5)
- Gandhi, S. P., Heeger, D. J., & Boynton, G. M. (1999). Spatial attention affects brain activity in human primary visual cortex. *Proceedings of the National Academy of Sciences*, *96*(6), 3314–3319. <https://doi.org/10.1073/pnas.96.6.3314>
- Goldfarb, E. V., Chun, M. M., & Phelps, E. A. (2016). Memory-Guided Attention: Independent Contributions of the Hippocampus and Striatum. *Neuron*, *89*(2), 317–324. <https://doi.org/10.1016/j.neuron.2015.12.014>
- Gorgolewski, K., Madison, C., Burns, C. D., Clark, D., Halchenko, Y. O., Waskom, M. L., & Ghosh, S. S. (2011). Nipype: A Flexible, Lightweight and Extensible Neuroimaging Data Processing Framework in Python. *Frontiers in Neuroinformatics*, *5*(August). <https://doi.org/10.3389/fninf.2011.00013>
- Greve, D. N., & Fischl, B. (2009). Accurate and robust brain image alignment using boundary-based registration. *NeuroImage*, *48*(1), 63–72. <https://doi.org/10.1016/j.neuroimage.2009.06.060>
- Günseli, E., & Aly, M. (2020). Preparation for upcoming attentional states in the hippocampus and medial prefrontal cortex. *eLife*, *9*, e53191. <https://doi.org/10.7554/eLife.53191>
- Hannula, D. E., & Ranganath, C. (2009). The Eyes Have It: Hippocampal Activity Predicts Expression of Memory in Eye Movements. *Neuron*, *63*(5), 592–599. <https://doi.org/10.1016/j.neuron.2009.08.025>
- Himmelberg, M. M., Kurzwaski, J. W., Benson, N. C., Pelli, D. G., Carrasco, M., & Winawer, J. (2021). Cross-dataset reproducibility of human retinotopic maps. *NeuroImage*, *244*, 118609. <https://doi.org/10.1016/j.neuroimage.2021.118609>
- Hindy, N. C., Ng, F. Y., & Turk-Browne, N. B. (2016). Linking pattern completion in the hippocampus to predictive coding in visual cortex. *Nature Neuroscience*, *19*(5), 665–667. <https://doi.org/10.1038/nn.4284>
- Hirschstein, Z., & Aly, M. (2023). Long-term memory and working memory compete and cooperate to guide attention. *Attention, Perception, & Psychophysics*, *85*(5), 1517–1549. <https://doi.org/10.3758/s13414-022-02593-1>
- Hulbert, J. C., & Norman, K. A. (2015). Neural differentiation tracks improved recall of competing memories following interleaved study and retrieval practice. *Cerebral Cortex*, *25*(10), 3994–4008. <https://doi.org/10.1093/cercor/bhu284>
- Hutchinson, J. B., & Turk-Browne, N. B. (2012). Memory-guided attention: Control from multiple memory systems. *Trends in Cognitive Sciences*, *16*(12), 576–579. <https://doi.org/10.1016/j.tics.2012.10.003>
- Jenkinson, M., Bannister, P., Brady, M., & Smith, S. (2002). Improved Optimization for the Robust

- and Accurate Linear Registration and Motion Correction of Brain Images. *NeuroImage*, 17(2), 825–841. <https://doi.org/10.1006/nimg.2002.1132>
- Jiang, J., Wang, S.-F., Guo, W., Fernandez, C., & Wagner, A. D. (2020). Prefrontal reinstatement of contextual task demand is predicted by separable hippocampal patterns. *Nature Communications*, 11, 2053. <https://doi.org/10.1038/s41467-020-15928-z>
- Kastner, S., Pinsk, M. A., De Weerd, P., Desimone, R., & Ungerleider, L. G. (1999). Increased activity in human visual cortex during directed attention in the absence of visual stimulation. *Neuron*, 22(4), 751–761. [https://doi.org/10.1016/S0896-6273\(00\)80734-5](https://doi.org/10.1016/S0896-6273(00)80734-5)
- Kastner, S., & Ungerleider, L. G. (2000). Mechanisms of visual attention in the human cortex. *Annual Review of Neuroscience*, 23, 315–341. <https://doi.org/10.1146/annurev.neuro.23.1.315>
- Kerrén, C., van Bree, S., Griffiths, B. J., & Wimber, M. (2022). Phase separation of competing memories along the human hippocampal theta rhythm. *eLife*, 11, e80633. <https://doi.org/10.7554/eLife.80633>
- Killian, N. J., Jutras, M. J., & Buffalo, E. a. (2012). A map of visual space in the primate entorhinal cortex. *Nature*, 491(7426), 761–764. <https://doi.org/10.1038/nature11587>
- Klein, A., Ghosh, S. S., Bao, F. S., Giard, J., Häme, Y., Stavsky, E., Lee, N., Rossa, B., Reuter, M., Neto, E. C., & Keshavan, A. (2017). Mindboggling morphometry of human brains. *PLOS Computational Biology*, 13(2), e1005350. <https://doi.org/10.1371/journal.pcbi.1005350>
- Kok, P., Jehee, J. F. M., & de Lange, F. P. (2012). Less Is More: Expectation Sharpens Representations in the Primary Visual Cortex. *Neuron*, 75(2), 265–270. <https://doi.org/10.1016/j.neuron.2012.04.034>
- Kok, P., & Turk-Browne, N. B. (2018). Associative prediction of visual shape in the hippocampus. *The Journal of Neuroscience*, 38(31), 0163–18. <https://doi.org/10.1523/JNEUROSCI.0163-18.2018>
- Kosslyn, S. M., Thompson, W. L., Kim, I. J., & Alpert, N. M. (1995). Topographical representations of mental images in primary visual cortex. *Nature*, 378(6556), 496–498. <https://doi.org/10.1038/378496a0>
- Kuhl, B. a, Dudukovic, N. M., Kahn, I., & Wagner, A. D. (2007). Decreased demands on cognitive control reveal the neural processing benefits of forgetting. *Nature Neuroscience*, 10(7), 908–914. <https://doi.org/10.1038/nn1918>
- Lanczos, C. (1964). A Precision Approximation of the Gamma Function. *Journal of the Society for Industrial and Applied Mathematics Series B Numerical Analysis*, 1(1), 86–96. <https://doi.org/10.1137/0701008>
- Li, H.-H., Sprague, T. C., Yoo, A. H., Ma, W. J., & Curtis, C. E. (2021). Joint representation of working memory and uncertainty in human cortex. *Neuron*, 109(22), P3699-3712.e6. <https://doi.org/10.1016/j.neuron.2021.08.022>
- Lindsay, G. W. (2020). Convolutional Neural Networks as a Model of the Visual System: Past, Present, and Future. *Journal of Cognitive Neuroscience*, 33(10), 2017–2031. https://doi.org/10.1162/jocn_a_01544
- Liu, T., Pestilli, F., & Carrasco, M. (2005). Transient Attention Enhances Perceptual Performance and fMRI Response in Human Visual Cortex. *Neuron*, 45(3), 469–477.

- <https://doi.org/10.1016/j.neuron.2004.12.039>
- Mao, D., Avila, E., Caziot, B., Laurens, J., Dickman, J. D., & Angelaki, D. E. (2021). Spatial modulation of hippocampal activity in freely moving macaques. *Neuron*, *109*(21), 3521–3534.e6. <https://doi.org/10.1016/j.neuron.2021.09.032>
- McAdams, C. J., & Maunsell, J. H. (1999). Effects of attention on orientation-tuning functions of single neurons in macaque cortical area V4. *The Journal of Neuroscience: The Official Journal of the Society for Neuroscience*, *19*(1), 431–441. <https://doi.org/10.1523/JNEUROSCI.19-01-00431.1999>
- Molitor, R. J., Sherrill, K. R., Morton, N. W., Miller, A. A., & Preston, A. R. (2020). Memory reactivation during learning simultaneously promotes dentate gyrus/CA2,3 pattern differentiation and CA1 memory integration. *Journal of Neuroscience*, *41*(4), 726–738. <https://doi.org/10.1523/JNEUROSCI.0394-20.2020>
- Nickel, A. E., Hopkins, L. S., Minor, G. N., & Hannula, D. E. (2020). Attention capture by episodic long-term memory. *Cognition*, *201*, 104312. <https://doi.org/10.1016/j.cognition.2020.104312>
- Nobre, A. C., & Stokes, M. G. (2019). Premembering Experience: A Hierarchy of Time-Scales for Proactive Attention. *Neuron*, *104*(1), 132–146. <https://doi.org/10.1016/j.neuron.2019.08.030>
- Norman, K. A., Newman, E., Detre, G., & Polyn, S. (2006). How inhibitory oscillations can train neural networks and punish competitors. *Neural Computation*, *18*, 1577–1610. <https://doi.org/10.1162/neco.2006.18.7.1577>
- O'Reilly, R. C., & McClelland, J. L. (1994). Hippocampal conjunctive encoding, storage, and recall: Avoiding a trade-off. *Hippocampus*, *4*(6), 661–682. <https://doi.org/10.1002/hipo.450040605>
- Poskanzer, C., & Aly, M. (2023). Switching between External and Internal Attention in Hippocampal Networks. *Journal of Neuroscience*, *43*(38), 6538–6552. <https://doi.org/10.1523/JNEUROSCI.0029-23.2023>
- Power, J. D., Mitra, A., Laumann, T. O., Snyder, A. Z., Schlaggar, B. L., & Petersen, S. E. (2014). Methods to detect, characterize, and remove motion artifact in resting state fMRI. *NeuroImage*, *84*, 320–341. <https://doi.org/10.1016/j.neuroimage.2013.08.048>
- Ritvo, V. J. H., Nguyen, A., Turk-Browne, N. B., & Norman, K. A. (2023). Differentiation and Integration of Competing Memories: A Neural Network Model. *eLife*, *12*. <https://doi.org/10.7554/eLife.88608>
- Ritvo, V. J. H., Turk-Browne, N. B., & Norman, K. A. (2019). Nonmonotonic Plasticity: How Memory Retrieval Drives Learning. *Trends in Cognitive Sciences*, *23*(9), 726–742. <https://doi.org/10.1016/j.tics.2019.06.007>
- Rolls, E. T. (1999). Spatial view cells and the representation of place in the primate hippocampus. *Hippocampus*, *9*(4), 467–480. [https://doi.org/10.1002/\(SICI\)1098-1063\(1999\)9:4<467::AID-HIPO13>3.0.CO;2-F](https://doi.org/10.1002/(SICI)1098-1063(1999)9:4<467::AID-HIPO13>3.0.CO;2-F)
- Rosen, M. L., Stern, C. E., Michalka, S. W., Devaney, K. J., & Somers, D. C. (2015). Influences of Long-Term Memory-Guided Attention and Stimulus-Guided Attention on Visuospatial Representations within Human Intraparietal Sulcus. *Journal of Neuroscience*, *35*(32), 11358–11363. <https://doi.org/10.1523/JNEUROSCI.1055-15.2015>
- Rosen, M. L., Stern, C. E., Michalka, S. W., Devaney, K. J., & Somers, D. C. (2016). Cognitive Control

- Network Contributions to Memory-Guided Visual Attention. *Cerebral Cortex*, 26(5), 2059–2073. <https://doi.org/10.1093/cercor/bhv028>
- Ruiz, N. A., Meager, M. R., Agarwal, S., & Aly, M. (2020). The Medial Temporal Lobe Is Critical for Spatial Relational Perception. *Journal of Cognitive Neuroscience*, 32(9), 1–16. https://doi.org/10.1162/jocn_a_01583
- Ryan, J. D., Althoff, R. R., Whitlow, S., & Cohen, N. J. (2000). Amnesia is a Deficit in Relational Memory. *Psychological Science*, 11(6), 454–461. <https://doi.org/10.1111/1467-9280.00288>
- Ryan, J. D., Shen, K., & Liu, Z.-X. (2020). The intersection between the oculomotor and hippocampal memory systems: Empirical developments and clinical implications. *Annals of the New York Academy of Sciences*, 1464(1), 115–141. <https://doi.org/10.1111/nyas.14256>
- Satterthwaite, T. D., Elliott, M. A., Gerraty, R. T., Ruparel, K., Loughhead, J., Calkins, M. E., Eickhoff, S. B., Hakonarson, H., Gur, R. C., Gur, R. E., & Wolf, D. H. (2013). An improved framework for confound regression and filtering for control of motion artifact in the preprocessing of resting-state functional connectivity data. *NeuroImage*, 64, 240–256. <https://doi.org/10.1016/j.neuroimage.2012.08.052>
- Schlichting, M. L., Mumford, J. A., & Preston, A. R. (2015). Learning-related representational changes reveal dissociable integration and separation signatures in the hippocampus and prefrontal cortex. *Nature Communications*, 6, 8151. <https://doi.org/10.1038/ncomms9151>
- Shapiro, M. L., & Olton, D. S. (1994). Hippocampal function and interference. In *Memory systems 1994* (pp. 87–117). The MIT Press.
- Somers, D. C., Dale, A. M., Seiffert, A. E., & Tootell, R. B. H. (1999). Functional MRI reveals spatially specific attentional modulation in human primary visual cortex. *Proceedings of the National Academy of Sciences*, 96(4), 1663–1668. <https://doi.org/10.1073/pnas.96.4.1663>
- Sprague, T. C., & Serences, J. T. (2013). Attention modulates spatial priority maps in the human occipital, parietal and frontal cortices. *Nature Neuroscience*, 16(12), 1879–1887. <https://doi.org/10.1038/nn.3574>
- Stokes, M. G., Atherton, K., Patai, E. Z., & Nobre, A. C. (2012). Long-term memory prepares neural activity for perception. *Proceedings of the National Academy of Sciences*, 109(6), E360–E367. <https://doi.org/10.1073/pnas.1108555108>
- Summerfield, J. J., Lepsien, J., Gitelman, D. R., Mesulam, M. M., & Nobre, A. C. (2006). Orienting attention based on long-term memory experience. *Neuron*, 49(6), 905–916. <https://doi.org/10.1016/j.neuron.2006.01.021>
- Tustison, N. J., Avants, B. B., Cook, P. A., Zheng, Y., Egan, A., Yushkevich, P. A., & Gee, J. C. (2010). N4ITK: Improved N3 Bias Correction. *IEEE Transactions on Medical Imaging*, 29(6), 1310–1320. <https://doi.org/10.1109/TMI.2010.2046908>
- van Moorselaar, D., & Slagter, H. A. (2020). Inhibition in selective attention. *Annals of the New York Academy of Sciences*, 1464(1), 204–221. <https://doi.org/10.1111/nyas.14304>
- Wammes, J., Norman, K. A., & Turk-Browne, N. (2022). Increasing stimulus similarity drives nonmonotonic representational change in hippocampus. *eLife*, 11, e68344. <https://doi.org/10.7554/eLife.68344>
- Wandell, B. A., & Winawer, J. (2015). Computational neuroimaging and population receptive fields. *Trends in Cognitive Sciences*, 19(6), 349–357. <https://doi.org/10.1016/j.tics.2015.03.009>

- Wandell, B., Dumoulin, S., & Brewer, A. a. (2007). Visual Field Maps in Human Cortex. *Neuron*, 56(2), 366–383. <https://doi.org/10.1016/j.neuron.2007.10.012>
- Wanjia, G., Favila, S. E., Kim, G., Molitor, R. J., & Kuhl, B. A. (2021). Abrupt hippocampal remapping signals resolution of memory interference. *Nature Communications*, 12, 4816. <https://doi.org/10.1038/s41467-021-25126-0>
- Wimber, M., Alink, A., Charest, I., Kriegeskorte, N., & Anderson, M. C. (2015). Retrieval induces adaptive forgetting of competing memories via cortical pattern suppression. *Nature Neuroscience*, 18(4), 582–589. <https://doi.org/10.1038/nn.3973>
- Wynn, J. S., Ryan, J. D., & Buchsbaum, B. R. (2020). Eye movements support behavioral pattern completion. *Proceedings of the National Academy of Sciences*, 117(11), 6246–6254. <https://doi.org/10.1073/pnas.1917586117>
- Yamins, D. L. K., Hong, H., Cadieu, C. F., Solomon, E. A., Seibert, D., & DiCarlo, J. J. (2014). Performance-optimized hierarchical models predict neural responses in higher visual cortex. *Proceedings of the National Academy of Sciences*, 111(23), 8619–8624. <https://doi.org/10.1073/pnas.1403112111>
- Zhang, Y., Brady, M., & Smith, S. (2001). Segmentation of brain MR images through a hidden Markov random field model and the expectation-maximization algorithm. *IEEE Transactions on Medical Imaging*, 20(1), 45–57. <https://doi.org/10.1109/42.906424>